The MIA complex is a conserved and novel dynein regulator essential for normal ciliary motility

Ryosuke Yamamoto,[1] Kangkang Song,[2] Haru-aki Yanagisawa,[3] Laura Fox,[1] Toshiki Yagi,[3] Maureen Wirschell,[1] Masafumi Hirono,[4] Ritsu Kamiya,[4] Daniela Nicastro,[2] and Winfield S. Sale[1]

[1]Department of Cell Biology, Emory University School of Medicine, Atlanta, GA 30322
[2]Department of Biology, Rosenstiel Science Center, Brandeis University, Waltham, MA 02454
[3]Department of Cell Biology and Anatomy, Graduate School of Medicine, and [4]Department of Biological Sciences, University of Tokyo, Tokyo 113-0033, Japan

Axonemal dyneins must be precisely regulated and coordinated to produce ordered ciliary/flagellar motility, but how this is achieved is not understood. We analyzed two *Chlamydomonas reinhardtii* mutants, *mia1* and *mia2*, which display slow swimming and low flagellar beat frequency. We found that the *MIA1* and *MIA2* genes encode conserved coiled-coil proteins, FAP100 and FAP73, respectively, which form the modifier of inner arms (MIA) complex in flagella. Cryo–electron tomography of *mia* mutant axonemes revealed that the MIA complex was located immediately distal to the intermediate/light chain complex of I1 dynein and structurally appeared to connect with the nexin–dynein regulatory complex. In axonemes from mutants that lack both the outer dynein arms and the MIA complex, I1 dynein failed to assemble, suggesting physical interactions between these three axonemal complexes and a role for the MIA complex in the stable assembly of I1 dynein. The MIA complex appears to regulate I1 dynein and possibly outer arm dyneins, which are both essential for normal motility.

Introduction

Motile cilia and flagella are complex microtubule-based organelles critical for embryonic development and organ functions (Satir and Christensen, 2007; Roy, 2009; Lee, 2011; Smith and Rohatgi, 2011). Ciliary motility is generated by the coordinated activities of both the axonemal outer dynein arms (ODAs) and inner dynein arms (IDAs), which are regulated in a precise spatial and temporal manner (Brokaw, 1994; Kamiya, 2002; King and Kamiya, 2009; Lindemann, 2011). Although the ODAs generate the main force for control of ciliary beat frequency, the IDAs mainly contribute to control of the size and shape of the ciliary bend, parameters referred to as waveform (Brokaw and Kamiya, 1987; King and Kamiya, 2009). Failure in proper coordination and regulation of the dyneins results in abnormal ciliary motility, which is implicated in a wide range of human diseases known as ciliopathies (Marshall, 2008; Hildebrandt et al., 2011; Drummond, 2012; Hirokawa et al., 2012; Oh and Katsanis, 2012). However, we have little understanding of the mechanisms that coordinate the activity among the different ciliary dynein arms or that regulate the activity of each dynein subform (Kamiya, 2002; Brokaw, 2009; Lindemann and Lesich, 2010; Mitchison and Mitchison, 2010).

Theoretical and experimental analyses have indicated the oscillatory movement of cilia is, in part, an inherent property of the dynein motors (Yagi et al., 1994; Shingyoji et al., 1998) and regulation by a mechanical feedback mechanism, in which axonemal curvature or distortion regulates dynein activity (Hayashibe et al., 1997; Brokaw, 2002, 2009; Morita and Shingyoji, 2004; Hayashi and Shingyoji, 2008; Lindemann, 2011). However, effective motility of cilia also requires precise control of beat frequency and waveform, through regulation of the ODA and IDA, respectively. At least five conserved, key

R. Yamamoto and K. Song contributed equally to this paper.

Correspondence to Winfield S. Sale: wsale@emory.edu

M. Wirschell's present address is Dept. of Biochemistry, University of Mississippi Medical Center, Jackson, MS 39216.

R. Kamiya's present address is Dept. of Life Science, Faculty of Science, Gakushuin University, Tokyo 171-8588, Japan.

Abbreviations used in this paper: CBB, Coomassie brilliant blue; CP, central pair; cryo-ET, cryo–electron tomography; CSC, calmodulin- and spoke-associated complex; DMT, doublet microtubule; DRB, 5,6-dichloro-1-b-D-ribofuranosylbenzimidazole; ESI, electrospray ionization; HC, heavy chain; IC, intermediate chain; IDA, inner dynein arm; LC, light chain; MIA, modifier of inner arms; MS, mass spectrometry; N-DRC, nexin–dynein regulatory complex; ODA, outer dynein arm; OIDL, outer–inner dynein linker; PKI, protein kinase inhibitor; pWT, pseudo–wild type; RS, radial spoke.

The Rockefeller University Press $30.00
J. Cell Biol. Vol. 201 No. 2 263–278
www.jcb.org/cgi/doi/10.1083/jcb.201211048

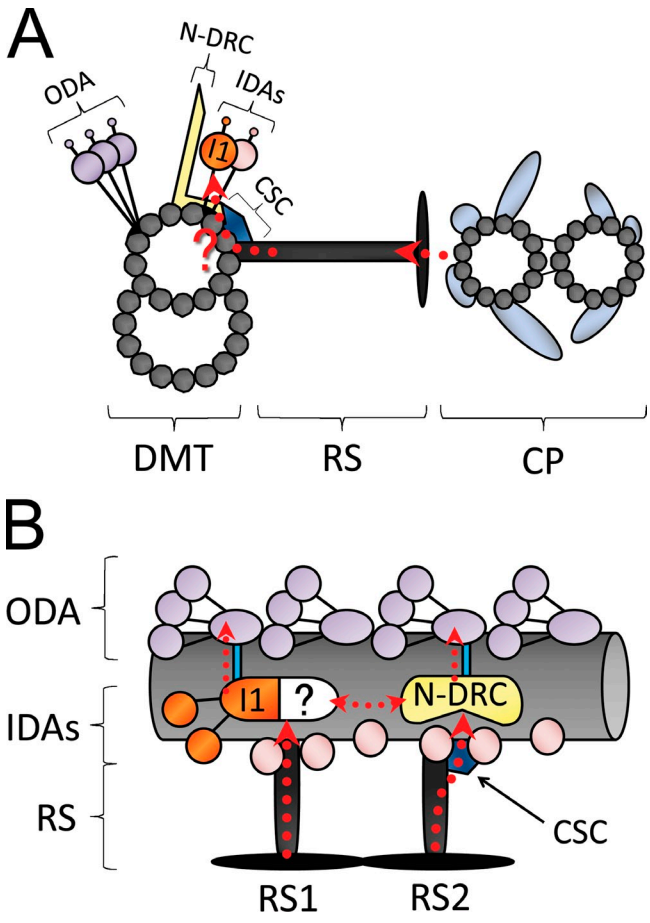

Figure 1. **Schematic model of motility regulation in *C. reinhardtii* axonemes.** (A and B) Models depicting mechanical/chemical signaling pathways (dotted red arrows) in *C. reinhardtii* axonemes. Transverse (A) and longitudinal (B) sections are shown. Based on genetic and pharmacological experiments, signals are transmitted from the CP, through the RS1 to I1 dynein, and through RS2 to the CSC and N-DRC. Signals are also thought to be transmitted from I1 dynein and N-DRC to ODAs through OIDLs (blue lines in B). The question addressed here is how signals are transmitted to I1 dynein (question marks in A and B).

axonemal complexes have been identified that regulate normal ciliary motility. They include the central pair (CP) apparatus, radial spokes (RSs), the nexin–dynein regulatory complex (N-DRC; Heuser et al., 2009), the calmodulin- and spoke-associated complex (CSC; Dymek et al., 2011; Heuser et al., 2012a), and the two-headed IDA called I1 dynein, also known as dynein f (Piperno, 1995; Porter and Sale, 2000). The regulatory mechanisms are thought to involve structural and chemical signals that begin in the CP and are then transmitted to the outer doublet microtubules (DMTs) by the RSs (Fig. 1, A and B; Smith and Yang, 2004). Although the composition and structure of the RSs have recently been revealed (Pigino et al., 2011; Lin et al., 2012a), how the RSs transmit signals to the outer DMTs is not understood.

The CSC, which is required for regulation of dynein and for calcium regulation of motility (Dymek et al., 2011; Heuser et al., 2012a), is associated with RS2 and the N-DRC in the distal region of the axonemal 96-nm repeat structure (Gardner et al., 1994; Heuser et al., 2009; Lin et al., 2011). Thus, the N-DRC and CSC are in perfect position to relay structural and/or chemical signals initiated in the CP and transmitted by the RSs to the dynein motors. However, despite recent detailed structural analyses showing physical connections between the N-DRC and CSC (Heuser et al., 2012a) and the N-DRC and dynein motors (Bui et al., 2008; Heuser et al., 2009), the mechanisms for regulation and signal transduction remain a mystery.

In the proximal part of the axonemal 96-nm repeat, the I1 dynein is the corresponding key regulator of dynein-driven microtubule sliding, relaying signals that are required for normal ciliary waveform (Wirschell et al., 2007; VanderWaal et al., 2011). I1 dynein is the only two-headed IDA, and the functional mechanism involves changes in phosphorylation of its regulatory intermediate chain (IC) IC138 by axonemal kinases and phosphatases (Gokhale et al., 2009; Elam et al., 2011) and is also regulated by the CP and RS (Smith and Yang, 2004). Based on additional genetic analysis (Porter et al., 1992) and measurement of microtubule sliding (Smith and Sale, 1992; Smith, 2002; Bower et al., 2009; Toba et al., 2011), the CP/RS structures also appear to regulate the ODAs, possibly mediated by I1 dynein (Kikushima, 2009). Consistent with this idea, recent cryo–electron tomography (cryo-ET) studies have revealed intriguing structural links between I1 dynein and the ODAs (Nicastro et al., 2006; Bui et al., 2008, 2012; Heuser et al., 2012b), possibly to coordinate activities between these dyneins. However, neither the proteins nor the functional roles of these linkers have been elucidated, nor have regulatory mechanisms that coordinate various axonemal dyneins been identified. One idea is that I1 dynein predominantly plays a regulatory role, like the N-DRC, controlling the activity of other dyneins (Kotani et al., 2007; Bower et al., 2009; Toba et al., 2011; Heuser et al., 2012b). However, the mechanism of transmission of signals from the RSs to I1 dynein and regulation of I1 dynein is not understood.

To further investigate the mechanism for how I1 dynein is regulated, we analyzed two *Chlamydomonas reinhardtii* motility mutants, *mia1* and *mia2*. The *mia* mutants were identified in genetic screens for cells with defects in axonemal dynein regulation (King and Dutcher, 1997). The mutants fail to perform normal phototaxis and display abnormal phosphorylation of IC138, indicative of a defect in regulation of I1 dynein and control of ciliary waveform (Bower et al., 2009; VanderWaal et al., 2011). Here, we report that the gene products of *mia1* and *mia2* are the conserved coiled-coil proteins, FAP100 and FAP73, respectively, that form a tight complex in the axoneme, which we named the modifier of inner arms (MIA) complex. Cryo-ET indicates that the MIA complex is localized to every 96-nm axonemal repeat just distal to the I1 dynein IC/light chain (LC) complex and proximal to the N-DRC. Biochemical data demonstrate that the MIA complex interacts with I1 dynein components, and structural data suggest that I1 dynein is structurally more flexible in the *mia* mutants. The *mia* mutants also display reduced ciliary beat frequencies indicative of defects in regulation of the ODAs. These results are consistent with the idea that the MIA complex functions in a regulatory pathway that controls the activities of I1 dynein and possibly of the ODAs.

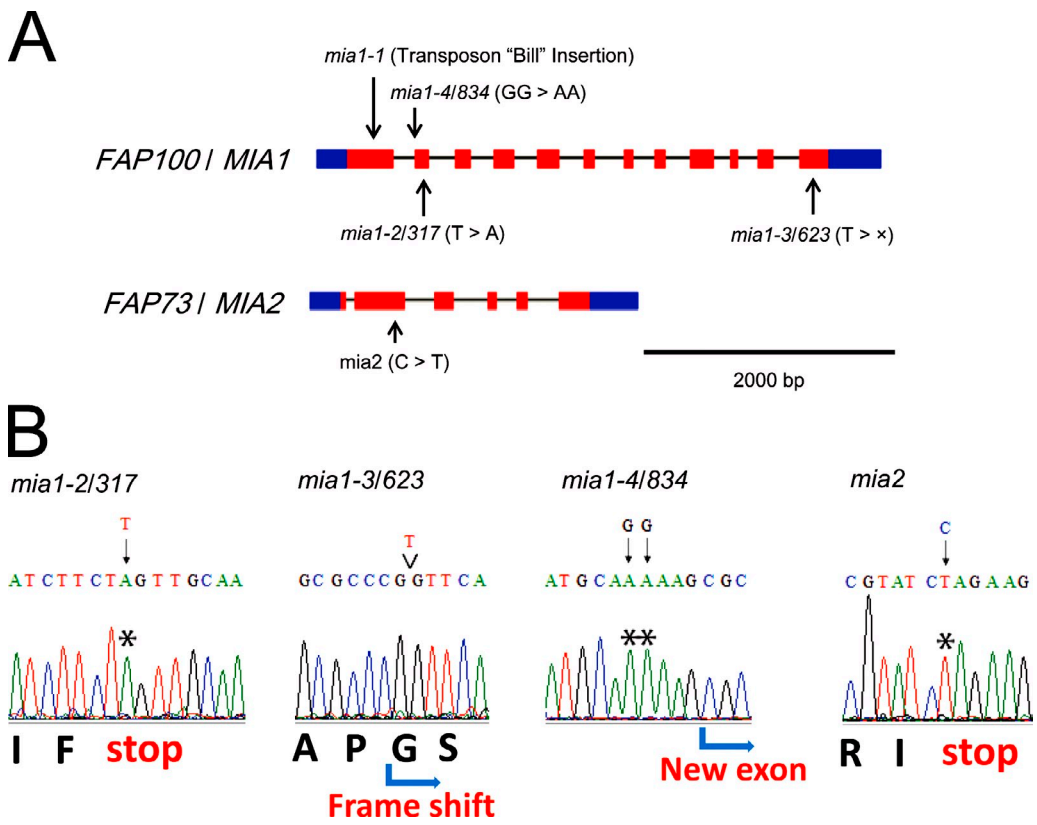

Figure 2. **The *MIA1* and *MIA2* genes in *C. reinhardtii* encode conserved coiled-coil proteins.** (A) The genomic structure of the *MIA1* and *MIA2* genes, showing untranslated regions in blue, exons in red, and introns as black lines. The mutations in the *mia1* alleles and *mia2* are indicated. (B) Sequence analyses of the *mia* mutants (*mia1-2/317*, *mia1-3/623*, *mia1-4/834*, and *mia2*) reveal the consequences resulting from the indicated mutations. Coloring indicates DNA bases (blue, cytosine; red, thymine; green, adenine; black, guanine). Asterisks indicate mutations sites.

Results

The *MIA1* gene encodes the coiled-coil protein FAP100

While searching for *C. reinhardtii* IDA-deficient mutants from our UV-mutagenized library (Kamiya et al., 1991), we isolated three motility mutants, 317, 623, and 834, which showed slightly jerky, slow-swimming phenotypes, reduced flagellar beat frequencies, and defective phototaxis. The mutations mapped to linkage group II/chromosome 2 near the previously mapped location for the *mia1* mutant (King and Dutcher, 1997). Of the candidate genes in this region, *FAP100* was of particular interest because it is highly conserved in organisms with motile cilia, and its predicted mass (65.2 kD with an isoelectric point of 5.37) is consistent with that previously reported for a protein missing in *mia1* (King and Dutcher, 1997). Sequence analysis revealed mutations in the *FAP100* gene for all three strains as well as the original *mia1*: strain 317 has a T to A substitution, which creates a premature stop at codon 127; strain 623 has a one-base deletion in codon 534 (GTG to GG), resulting in a frame shift mutation; and strain 834 has a two-base (GG to AA) substitution, which alters the 5′ splice site of exon 2 (Fig. 2, A and B). The original *mia1* mutant (King and Dutcher, 1997) has the ∼560-bp "Bill" transposon (Kim et al., 2006) inserted in the first exon of *FAP100*, resulting in failure of expression of this protein (Fig. 3 A). Because 317, 623, and 834 are alleles of *mia1*, we renamed the original *mia1* to *mia1-1*, 317 to *mia1-2*, 623 to *mia1-3*, and 834 to *mia1-4*. We made an antibody against the FAP100 protein (Fig. S1), and immunoblotting revealed that FAP100 is missing from axonemes from all three of these strains as well as the original *mia1-1* (Fig. 3 A). Using the wild-type *FAP100* genomic fragment with a triple HA (3×HA) tag at the C terminus of the coding region, we rescued the *mia1* phenotype. The rescued strain, *mia1R*, had nearly wild-type motility and phototaxis (unpublished data). Furthermore, immunoblot analysis revealed that FAP100-HA is assembled in the axonemes from *mia1R* (Fig. 3 B). The data definitively reveal that *MIA1* encodes FAP100.

FAP100/Mia1p interacts with the coiled-coil protein FAP73/Mia2p to form the MIA complex

To identify FAP100-interacting proteins, we immunoprecipitated FAP100-HA from high salt extracts derived from *mia1R* axonemes using anti-HA antibodies (Fig. 3 C). Comparison between precipitates from *mia1R* and wild type, which does not express HA-tagged FAP100, clearly identified an ∼76-kD protein and an ∼35-kD protein that were exclusively pulled down in precipitates from *mia1R* extracts. Mass spectrometry (MS) analysis revealed the 76-kD band to be FAP100-HA and the 35-kD band to be FAP73. Both are coiled-coil proteins (Fig. 3 D) conserved in organisms with motile cilia and flagella.

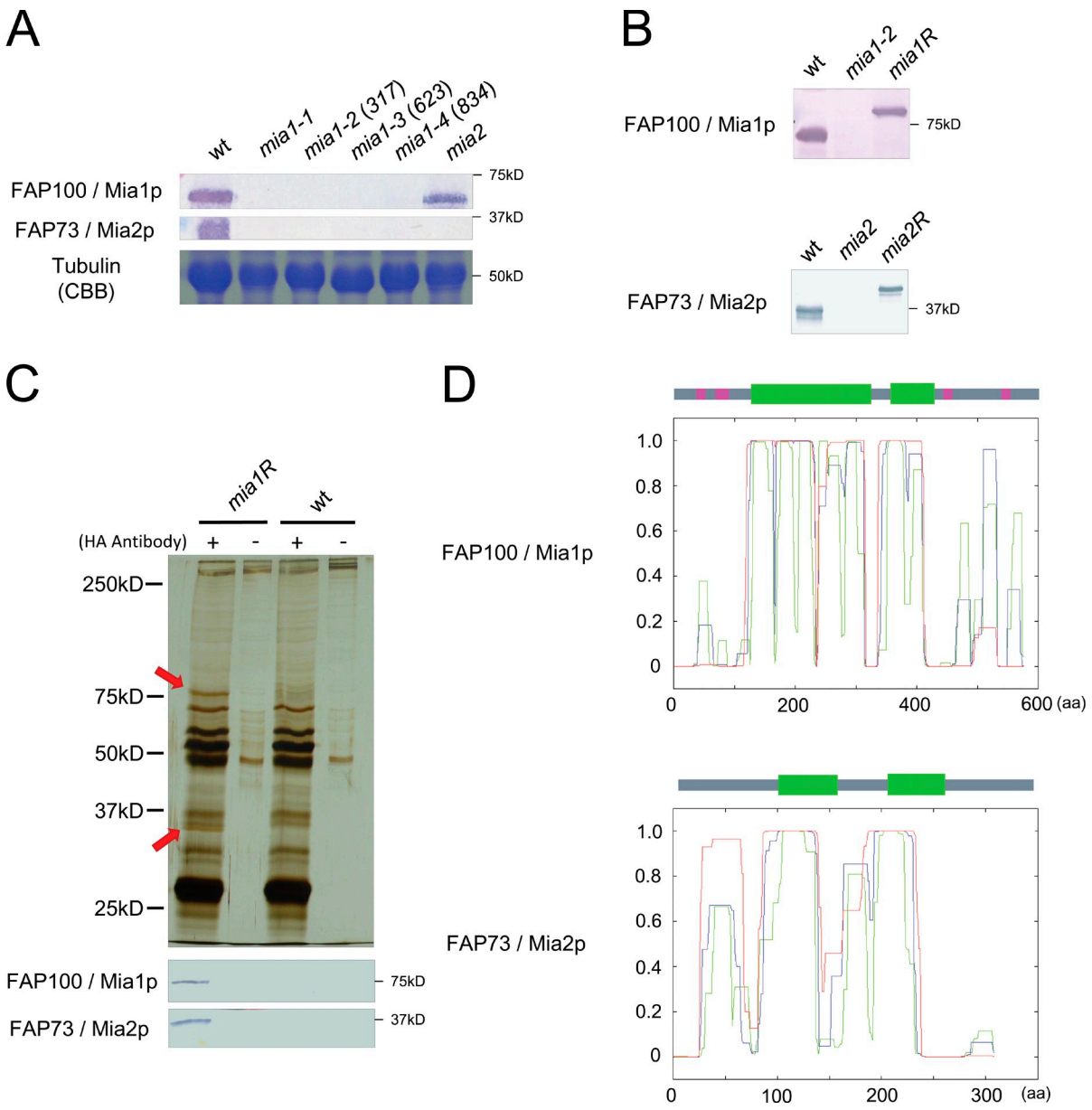

Figure 3. **The Mia1 and Mia2 proteins form the MIA complex.** (A) Anti-FAP100 and -FAP73 antibodies detect bands in wild-type axonemes. Both bands are missing or greatly reduced in *mia1*, whereas only the FAP73 band is missing in *mia2*. CBB staining of tubulin from each sample is shown as a loading control. (B) Axonemes from HA-tagged rescued strains (*mia1R* and *mia2R*) assemble FAP100 (top) and FAP73 (bottom). The expressed proteins have slower migration as a result of the expression of the 3×HA tags. (C) Immunoprecipitations from *mia1R* extracts using the anti-HA antibody pull down an ∼76-kD protein (FAP100-HA) and an ∼35-kD protein (FAP73; both indicated by red arrows). Plus and minus signs indicate addition of beads with or without the anti-HA antibody. Immunoblots using the specific antibodies also show that these proteins were precipitated only in the *mia1R* extracts. (D) The Mia1p (FAP100; top) and Mia2p (FAP73; bottom) domain structures were predicted using the SMART and COILS programs. Both proteins show a high probability of forming coiled-coil domains in the middle part of the protein. The color coding in the structure prediction by SMART analysis: green, regions having a high probability of forming coiled-coil structure; pink, regions of low complexity; gray, areas with no detectable domains. The window width in the structure prediction by COILS version 2.2: green, 14 residues; blue, 21 residues; red, 28 residues. wt, wild type.

The molecular mass of FAP73 (35.6 kD with an isoelectric point of 5.65) is consistent with that determined for a protein greatly reduced in *mia1* axonemes (King and Dutcher, 1997).

FAP73 maps to linkage group XVIII/chromosome 16 near the map position for the *mia2* mutant (King and Dutcher, 1997). Like *mia1*, *mia2* displays highly phosphorylated forms of IC138 in the axoneme (King and Dutcher, 1997). In *mia2*, the *FAP73* gene has a one-base substitution (C to T), resulting in a premature stop at codon 105 (Fig. 2, A and B). An antibody to FAP73 (Fig. S1) confirmed that FAP73 is missing from *mia2* axonemes (Figs. 3 A and 4 A), demonstrating that *mia2* is a null allele. We rescued the phototaxis and motility defects (not depicted) in *mia2* with a HA-tagged FAP73 protein (*mia2R*; Fig. 3 B). The data definitively reveal that *MIA2* encodes FAP73.

Although FAP100 and FAP73 are both absent or greatly reduced from *mia1* axonemes, FAP100 is present in *mia2* axonemes (Figs. 3 A and 4 A). Based on the coimmunoprecipitation and other biochemical data, FAP100 and FAP73 form an

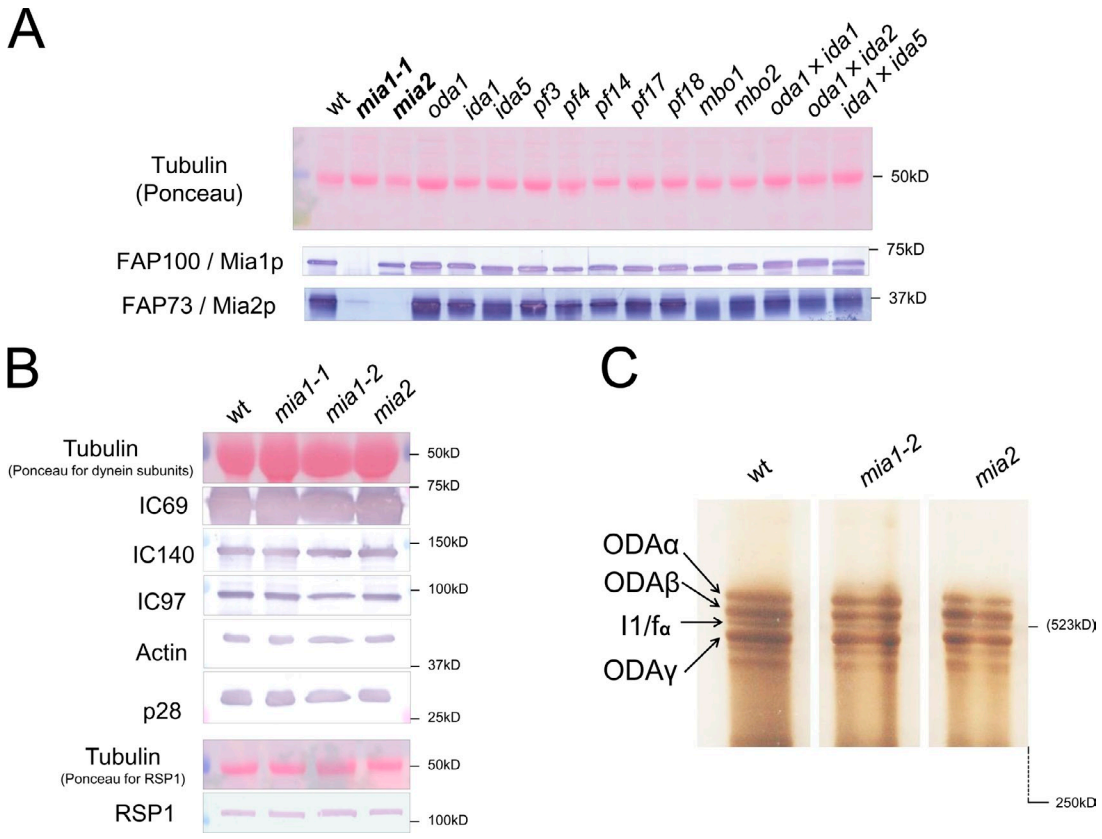

Figure 4. **FAP100 and FAP73 assemble in various motility mutants and the *mia* mutants contain ODAs and IDAs.** (A) Both FAP100 and FAP73 assemble in mutant axonemes that are missing the ODAs (*oda1*), I1 dynein (*ida1*), the single-headed IDAs a, c, d, and e (*ida5*), the N-DRC (*pf3*), the PP2A phosphatase (*pf4*), the RSs (*pf14 and pf17*), the CP (*pf18*), and the beaklike structures (*mbo1* and *mbo2*). The proteins are also present in double mutants (*oda1* × *ida1*, *oda1* × *ida2*, and *ida1* × *ida5*). (B) Immunoblots of subunits of the ODAs (IC69), I1 dynein (IC140 and IC97), the single-headed IDAs (actin and p28), and the RSs (RSP1) indicate these axonemal structures are apparently normal in both *mia1* and *mia2*. The dynein subunits were detected on a single gel and blot, and RSP1 was detected on a second gel and blot. Ponceau staining of tubulin is shown as a loading control for each gel. (C) Silver-stained 3–5% urea gel of isolated axonemes demonstrates that dynein HC composition appears unaltered in *mia* mutants relative to wild type. Three lanes are from the same gel. The predicted molecular mass of I1 dynein HCs is the expected value: dynein HCs migrate significantly more slowly than the 250-kD molecular mass marker, which is shown well below the region of the gel shown. wt, wild type.

axonemal complex, which we call the MIA complex after the names of original *C. reinhardtii* mutants. The stoichiometry of FAP100 and FAP73 in the MIA complex was estimated to be 1:1.83–2.89 from exponentially modified protein abundance index scores in our MS analysis and 1:2.53 from numbers of peptides per molecular weight observed in the *C. reinhardtii* proteome (Pazour et al., 2005).

The MIA complex localizes to the outer DMTs

To determine where the MIA complex localizes, we performed immunoblotting experiments using mutants lacking specific axonemal structures (Fig. 4 A). The MIA complex was present in axonemes defective in the CP (*pf18*), RS (*pf14* and *pf17*), ODA (*oda1*), I1 dynein (*ida1*), single-headed inner arms (*ida5*), the N-DRC (*pf3*), beak structures (*mbo1* and *mbo2*), and the protein phosphatase PP2A (*pf4*). Double mutants *oda1* × *ida1*, *oda1* × *ida2*, and *ida1* × *ida5* also had normal amounts of FAP100 and FAP73. Thus, the MIA complex is located on the outer DMTs.

Given the slow-swimming phenotype of *mia* strains, we analyzed *mia* mutant axonemes for the presence of other notable axonemal structures. Biochemical analyses indicate that *mia* mutant axonemes have normal amounts of outer arms (IC69), single-headed inner arms (p28 and actin), RS (RSP1; Fig. 4 B), and a normal dynein heavy chain (HC) profile (Fig. 4 C). In addition, assembly of I1 dynein (HCs, IC140, and IC97) in *mia* mutants appeared relatively normal (Fig. 4, B and C), although there are slight differences from culture to culture and allele to allele. Furthermore, the *mia* mutants manifest a highly phosphorylated IC138 (Fig. 5 A) consistent with a previous study (King and Dutcher, 1997), suggesting a defect in I1 dynein regulation. However, immunoblots indicate normal levels of signaling components (CK1, PP1, and PP2A; Fig. 5 B) important in the CP–RS pathway that regulates phosphorylation of IC138 (e.g., Gokhale et al., 2009; Elam et al., 2011). Thus, failure in assembly of the MIA complex does not result in failure of assembly of other axonemal proteins, including the kinases and phosphatases that regulate I1 dynein.

The MIA complex interacts with I1 dynein in the axoneme

To identify proteins that interact with the MIA complex in the axoneme, we used chemical cross-linking with EDC (1-ethyl-3-[3-dimethylaminopropyl] carbodiimide hydrochloride) followed

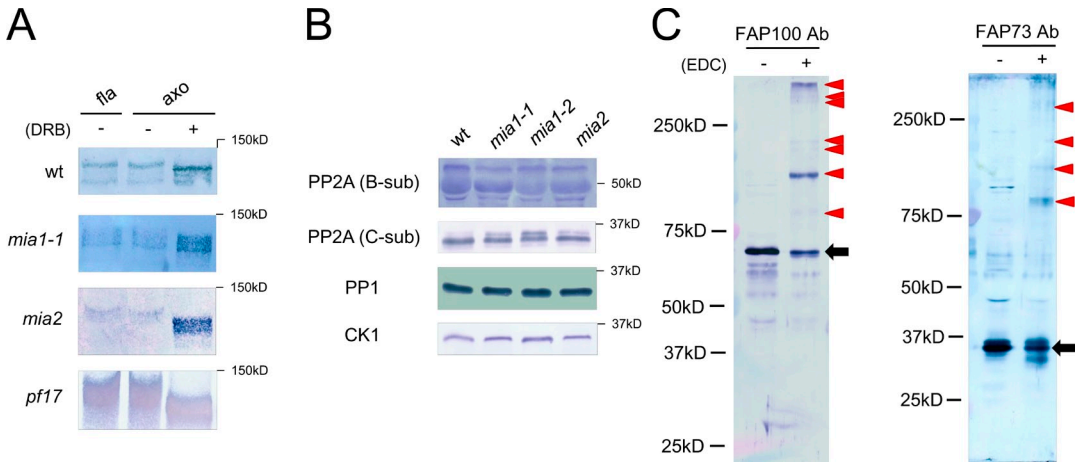

Figure 5. **The MIA complex functions in the I1 dynein phosphoregulatory pathway and interacts with multiple axonemal proteins.** (A) Untreated flagella (fla), untreated axonemes (axo), and axonemes treated with the kinase inhibitor DRB were probed with the anti-IC138 antibody. In the *mia* untreated axonemes, IC138 migrates in multiple forms in a manner similar to *pf17*. In contrast, wild-type axonemes show a compact IC138 profile. DRB treatment results in a shift in migration of IC138, indicating that these multiple forms of IC138 are caused by phosphorylation. (B) Immunoblot analyses indicate that CK1, PP2A (B and C subunits [sub]), and PP1 are assembled normally in the *mia* mutants. (C) Isolated wild-type axonemes treated with or without 5 mM EDC were probed with the FAP100 and FAP73 antibodies. Upon EDC exposure, both Mia proteins form some cross-linked products (red arrowheads), indicating that the MIA complex is in direct contact with multiple axonemal proteins. We could not detect the cross-linked products between I1 dynein subunits and the Mia proteins as solid bands on these blots. Black arrows indicate the un–cross-linked FAP100 and FAP73. Ab, antibody; wt, wild type.

by immunoprecipitation and identification by electrospray ionization (ESI)/liquid chromatography/MS/MS. Both FAP100 and FAP73 form cross-linked products in the axoneme upon exposure to EDC (Fig. 5 C). Using the rescued strains (*mia1R* and *mia2R*) and anti-HA antibodies for immunoprecipitation, I1 dynein HCs α and β and IC138 were precipitated from *mia1R*, and I1 dynein HC-β and IC138 were precipitated from *mia2R* (Table S1), strongly suggesting that the MIA complex physically interacts with IC138 and/or I1 dynein HCs. In addition to I1 dynein components, several other axonemal proteins were identified as potential components of the MIA complex (Table S1). Although the *mia* mutants display altered IC138 phosphorylation, no apparent kinase or phosphatase was precipitated with either FAP100-HA or FAP73-HA.

Cryo-ET reveals that the MIA complex is located distal to the IC/LC complex of I1 dynein, possibly extending across the middle of the 96-nm repeat to the N-DRC

Immunofluorescence of nucleoflagellar apparatuses from *mia1R* clearly showed that FAP100 is present along the entire length of both cilia, which is the same localization pattern obtained for I1 dynein (Fig. 6 A; Bui et al., 2012). To definitively determine structural changes and to localize the MIA complex, we used cryo-ET and subtomogram averaging of the 96-nm axonemal repeat to analyze the 3D structures of *mia* axonemes and compare them with pseudo–wild type (pWT) and *pf9-3/ida1* (Videos 1 and 2). Consistent with our EDC cross-linking results (Fig. 5 C and Table S1), cryotomographic averages of both *mia1* and *mia2* axonemes revealed structural defects in the distal portion of the I1 dynein IC/LC complex and in the structure located between I1 dynein and the N-DRC (Figs. 6, B and C; and S2, A–C; and Videos 3, 4, and 5). These structural defects are more severe in *mia1* than in *mia2*, supporting our biochemical results that *mia1* axonemes lack both FAP100 and FAP73, whereas *mia2* lacks only FAP73. Consistent with our biochemical analysis (Fig. 4, B and C), other structures including the RSs, N-DRC, and the dynein structures appear fully assembled as in the pWT control (Figs. 6, B and C; and S2, A–C; and Videos 1, 3, and 4).

Consistent with previous data (Nicastro et al., 2006; Bower et al., 2009; Heuser et al., 2012b), axonemes of the *pf9-3/ida1* mutant lack the entire I1 dynein, including the distal portion of the IC/LC complex that is reduced in the *mia* mutants. In contrast, the structure that bridges between the I1 dynein and N-DRC, which is missing or greatly reduced in the *mia* mutants, is present in *pf9-3/ida1* and pWT axonemes (Figs. 6 C and S2, A–C; and Videos 1, 2, 3, 4, and 5). Therefore, failure in I1 dynein assembly does not alter assembly of the MIA complex.

The MIA complex is important for the stable attachment of I1 dynein to the axoneme

The majority of the I1 dynein density is present in *mia* mutants, but we observed by cryo-ET that the density of the I1 dynein appeared weaker and blurred compared with pWT (Figs. 6 B and S2, A–C). This blurring was only observed for the I1 dynein and not for other axonemal structures. The blurred density of I1 dynein in the *mia* averages indicates heterogeneity between the averaged axonemal repeats, either because of assembly or positional differences, leading to bad alignment of just the I1 dynein in relation to the other axonemal structures. Classification of all averaged subtomogram volumes concerning presence or absence of the I1 dynein detected only occasional missing of the I1 dynein, mostly in random 96-nm repeats of both *mia* mutants (unpublished data). To test whether the position of I1 dynein is more flexible in *mia* axonemes than in wild type, we calculated local averages of the I1 dynein by masking

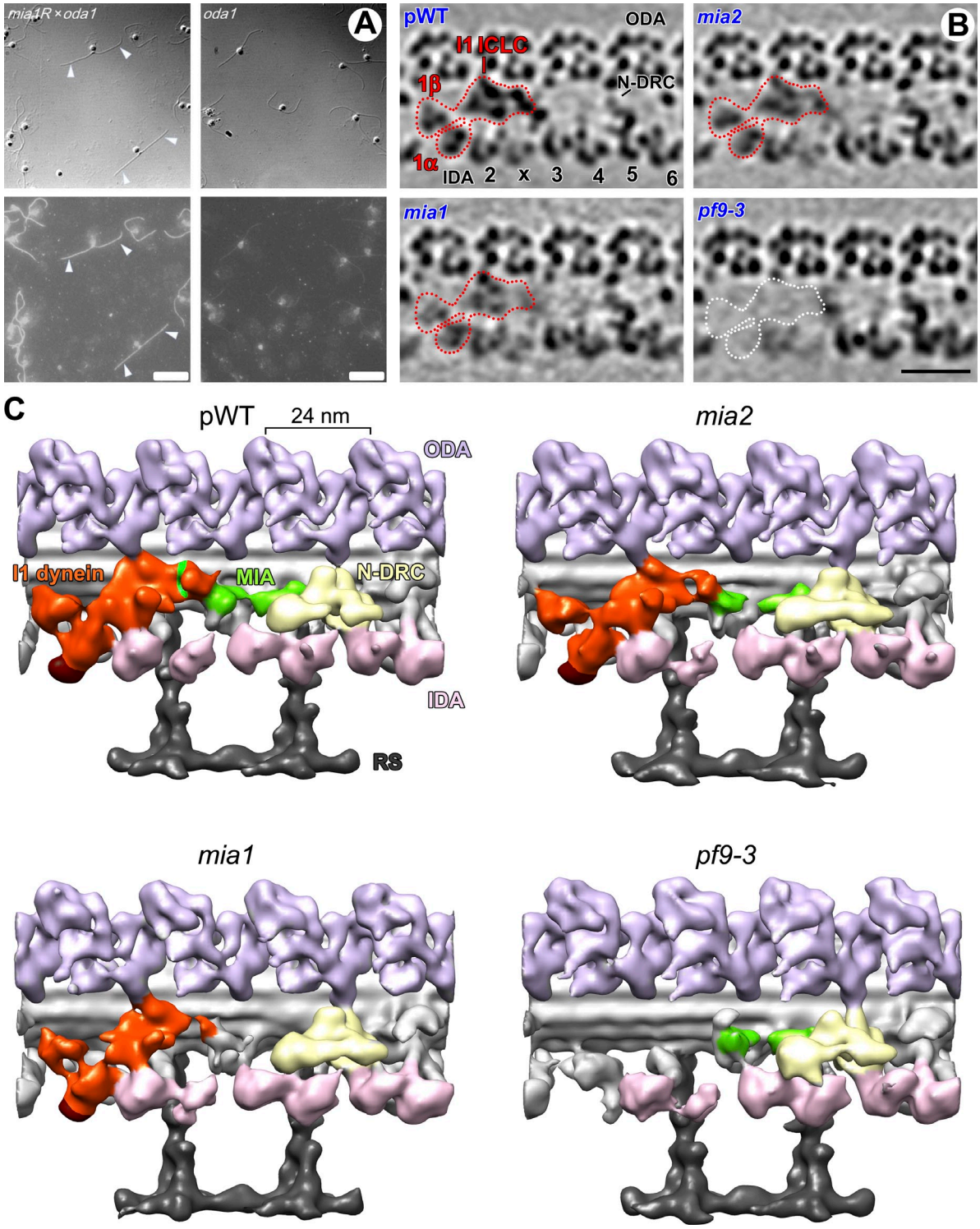

Figure 6. **The MIA complex is localized to a unique position in each 96-nm repeat.** (A) Nucleoflagellar apparatuses from *oda1* and *mia1R* × *oda1* were stained with the anti-HA antibody. The HA antibody detects FAP100-HA in both flagella in the *mia1R* × *oda1* strain (fluorescence image on the bottom). Very weak or no signal was detected in *oda1* flagella that do not express the FAP100-HA protein. Both basal bodies and nuclei have some nonspecific staining. (top) Differential interference contrast images show that all cells possess flagella. Arrowheads indicate cis- and trans-flagella, showing that both flagella are staining. (B) Longitudinal tomographic slices of the averaged 96-nm axonemal repeats from DMTs 1–9 of pWT, *mia2*, *mia1*, and *pf9-3/ida1* reveal structural defects in the mutant axonemes. The density of the I1 dynein (red outlines) is completely missing in *pf9-3/ida1* (white outlines) and appears reduced in the *mia* mutants. These defects are more prominent in *mia1* than in *mia2*. The densities of other major axonemal structures, such as the ODAs, single-headed inner dynein arms (IDAs 2–6 and X), and the N-DRC are not significantly changed in the *mia* mutants. (C) 3D isosurface renderings of the averaged 96-nm axonemal repeats from pWT, *mia2*, *mia1*, and *pf9-3/ida1* reveal the structural defects in more detail. Regions that are reduced in the *mia* averages are colored green; the most obvious defects are the distal density of the IC/LC of I1 dynein (orange) and the density between the I1 dynein and the N-DRC (yellow), which is reduced in *mia2*, missing in *mia1*, but fully assembled in pWT and *pf9-3/ida1*. The pWT and *pf9-3/ida1* data were refined from data originally reported by Heuser et al. (2012b). Proximal is on the left in B and C. Bars: (A) 10 µm; (B) 25 nm.

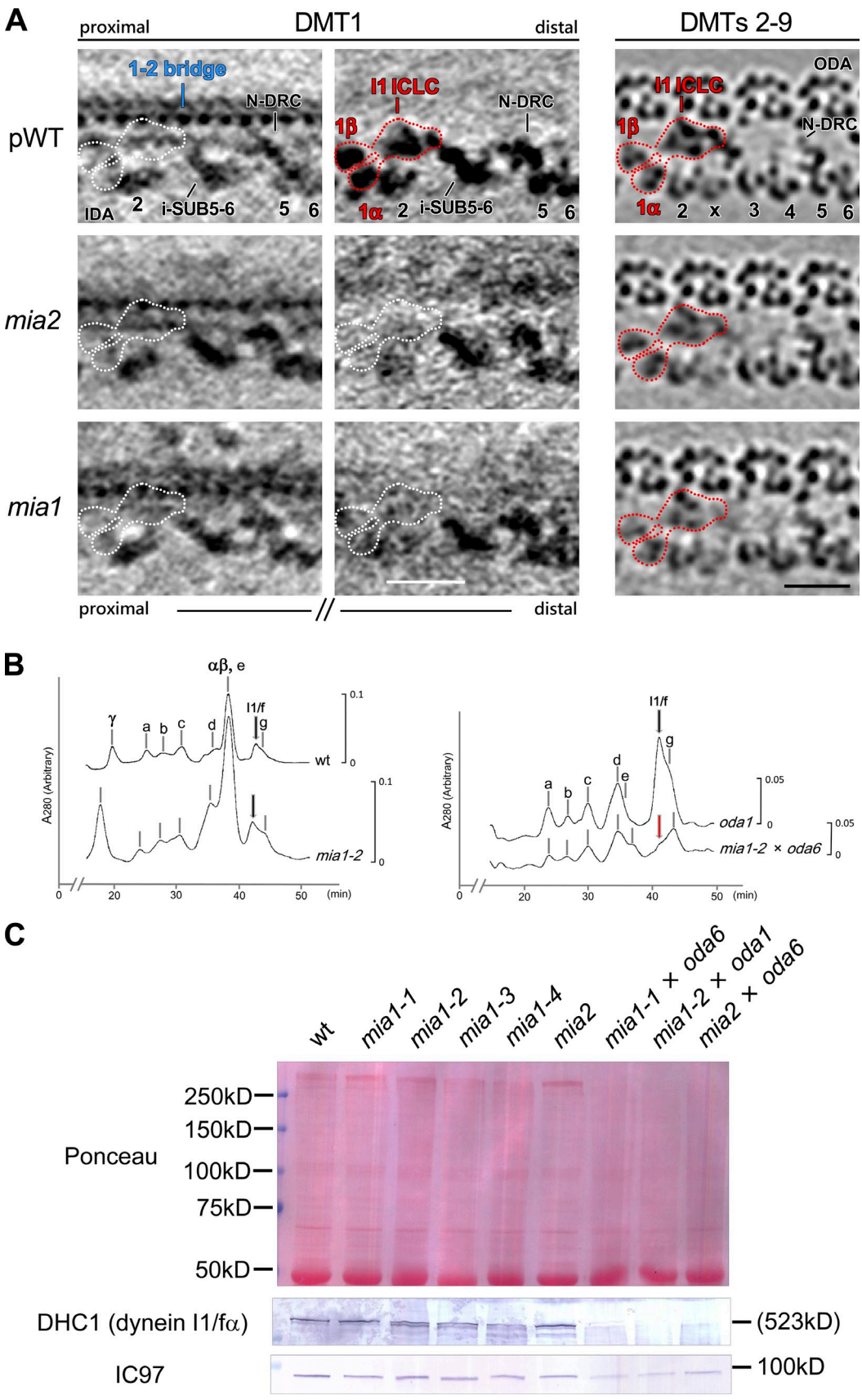

Figure 7. **The MIA complex affects I1 dynein stability in the axoneme.** (A) I1 dynein is missing along the entire length of DMT1 in the *mia* mutants. Tomographic slices of axonemal average of individual outer DMTs from pWT (top row), *mia2* (middle row), and *mia1* (bottom row). The first two columns show the axonemal repeat of DMT1 in the proximal (left) and distal (middle) regions; the right column depicts the combined average of the axonemal

all other structures during the alignment process. In contrast to the global averages in which the alignment is dominated by the density of the DMTs and other structures in the 96-nm repeat, in the local average of both *mia1* and *mia2*, the density of the I1 dynein appears very similar to the density in pWT, whereas the surrounding axonemal structures are greatly blurred because of alignment errors (unpublished data). This suggests that the I1 dynein density in the *mia* averages is mostly reduced because the position of the I1 dynein is more variable in the *mia* mutants than in pWT, which is consistent with a structural interaction between I1 dynein and the MIA complex.

In addition, doublet-specific averaging revealed an intriguing feature of *mia* mutant axonemes (Figs. 7 A and S3). DMTs 2–9 assemble all the IDA and ODA structures, and the defects noticeable are the missing densities distal of I1 dynein as described in the previous paragraph. Doublet-specific averages of DMTs 2–9 did not reveal obvious differences between these doublets in regards to the structural defects found in the *mia* mutants (Fig. S3). However, DMT1 of *mia1* and *mia2* axonemes shows additional defects compared with pWT. In wild-type *C. reinhardtii* flagella, DMT1 is known to exhibit unique features compared with DMTs 2–9: (a) the ODAs and the outer–inner dynein linkers (OIDLs) are missing along the entire length of DMT1, (b) in the proximal quarter of the flagellum, the ODAs are substituted by the 1–2 bridge that links DMTs 1 and 2 (Fig. 7 A; Hoops and Witman, 1983; Bui et al., 2009, 2012; Lin et al., 2012b), and (c) in the proximal region where the 1–2 bridge is present, the I1 dynein is missing (Bui et al., 2012; Lin et al., 2012b). In the *mia* mutants, however, I1 dynein is missing along the entire length of DMT1.

The results suggested that the MIA complex is located on all outer doublets (Fig. S3). However, one interpretation of the doublet-specific *mia* mutant defect is that I1 dynein assembly and stability are dependent on assembly of both the ODAs and the MIA complex, with the ODAs missing from DMT1. To test this, we used protein fractionation and immunoblots to compare the amount of I1 dynein assembled in axonemes from a *mia1* × *oda6* double mutant (lacking the MIA complex and ODAs) to *oda1* or *oda6* lacking only the ODAs. Chromatographic separation of flagellar dyneins revealed that the amount of I1 dynein is indeed reduced in axonemes from *mia1* × *oda6* compared with that of *oda1* (Fig. 7 B). In addition, immunoblots using antibodies to the I1 dynein HC and IC97 revealed a similar reduction of I1 dynein in other *mia* × *oda* double mutants (Fig. 7 C). These results indicate that I1 dynein assembly fails when both the ODA and MIA complex are missing and is dependent on both structures. Among these two stabilizing complexes, the MIA complex seems to be more crucial for stable I1 dynein assembly because, in contrast to the MIA complex, the absence of ODAs alone does not cause increased flexibility of the I1 dynein (Fig. 7 A, distal portion of DMT1 in pWT).

The MIA complex controls ciliary/flagellar motility through regulation of dynein activity

The *mia* mutants were first isolated as slow-swimming, non-phototactic cells (King and Dutcher, 1997). These are motility phenotypes common to defective I1 dynein assembly or regulation (Okita et al., 2005; Elam et al., 2011; VanderWaal et al., 2011) and that display excessive phosphorylated forms of IC138 (King and Dutcher, 1997). These observations are consistent with a role for the MIA complex in regulation of I1 dynein. In addition, from our analyses, the *mia* mutants have both swimming speed (~60 µm/s) and beat frequency (40–50 Hz) defects (Fig. S4 and Table 1) that are more severe than those observed for I1 dynein mutants (swimming velocity: ~100 µm/s; beat frequency: ~60 Hz; Table 1; Hendrickson et al., 2004; VanderWaal et al., 2011), indicating that the MIA complex may regulate multiple dyneins, including direct or indirect regulation of the ODAs.

To test whether the MIA complex regulates the function of more than one species of axonemal dynein, we analyzed motility in a series of *C. reinhardtii* double mutants defective in both the MIA complex and selected dynein arms. As expected, doubles between *mia* mutants (*mia1* × *mia2*) and I1 dynein–deficient mutants (*mia1* × *ida1*, *mia1* × *ida2*, *mia1* × *bop5*, and *mia2* × *bop5*) showed quite similar motility phenotypes to those of *mia* alone (Fig. S4 and Table 1). These results strongly suggest a functional interaction between the MIA complex and I1 dynein and indicate that the I1 dynein is inactive in the *mia* mutants (see Discussion). The double mutants between the *mia* mutants and *ida4* (lacking dynein a, c, and d), *ida6* (lacking dynein e and having a defect in N-DRC; Porter, 2011), and *ida9* (lacking dynein c) all showed more severe motility phenotypes (nearly nonmotile) than either parent (Table I). Similarly, doubles between the *mia* mutants and *oda* mutants show very low beat frequencies (10–20 Hz), indicating a more severe phenotype than either parent (Fig. S4 and Table I). These results indicate that the MIA complex operates in the same pathway as I1 dynein but that the MIA

repeats from DMTs 2–9 that do not show obvious structural differences between the proximal and distal regions (for individual DMT averages, see Fig. S3). In wild type, I1 dynein is missing from the proximal region of DMT1 (white outlines) but is present in the distal region (red outlines). In contrast, in both *mia* mutants, I1 dynein is missing along the entire length of DMT1 (white outlines). The pWT data were refined from data originally reported by Heuser et al. (2009) and Lin et al. (2012b). Other structures labeled are single-headed inner dynein arms (IDAs 2–6 and X), the N-DRC, and the inner SUB5-6 bridge. Bars, 25 nm. (B) Representative ion-exchange chromatography (Mono Q; GE Healthcare) elution profiles of axonemal dyneins show that I1 dynein levels (black arrows) appear relatively normal in *mia1-2* extracts compared with that of wild-type extracts (left graph), consistent with the immunoblotting results using I1 dynein subunit antibodies (Fig. 4 B). In contrast, I1 dynein is drastically reduced in the *mia1-2* × *oda6* double mutant (red arrow) compared with the *oda1* single mutant (right graph), suggesting that I1 dynein becomes unstable without both ODAs and the MIA complex. Typical Mono Q elution patterns are shown (A280 protein estimate in arbitrary units is indicated to the right of each scan [y axis]; elution time in minutes is shown on the x axis), and at least two experiments were performed for each strain. Elution of dynein complexes began at ~12 min. (C) Immunoblot analysis of isolated axonemes using the anti-DHC1 (I1 dynein HC-α) and IC97 antibodies confirms the reduction of I1 dynein in *mia* × *oda* double mutants. I1 dynein appears normal to slightly reduced in the single *mia* mutants relative to wild type (wt).

Table 1. **Phenotypes of the *mia* mutants**

Mutant	Defect	Phenotype	Typical beat frequency
			Hz
Wild type	None	Slightly jerky or smooth, fast swimming	60–70
mia1-1	MIA complex	Slightly jerky, slow swimming	40–50
mia1-2			
mia1-3			
mia1-4			
mia2	MIA complex	Slightly jerky or jerky (some cells), slow swimming	∼40
mia1-1 × mia2	MIA complex	Slightly jerky or jerky (some cells), slow swimming (similar to *mia*)	40–50
mia1-1 × bop5-4	MIA complex; IC138 complex	Slightly jerky or smooth (some cells), slow swimming (similar to *mia*)	40–50
mia1-3 × ida1	MIA complex; I1 dynein	Slightly jerky or smooth (some cells), slow swimming (similar to *mia*)	40–50
mia1-2 × ida2	MIA complex; I1 dynein	Slightly jerky or smooth (some cells), slow swimming (similar to *mia*)	40–50
mia1-2 × ida4	MIA complex; dynein a, c, and d	Nearly nonmotile (more severe than *mia*)	<10
mia1-4 × ida4	MIA complex; dynein a, c, and d	Nearly nonmotile (more severe than *mia*)	<10
mia1-1 × ida9	MIA complex; dynein c	Nonmotile or beat at very low beat frequency (more severe than *mia*)	<10
mia1-2 × oda1	MIA complex; ODA	Beat at very low beat frequency (more severe than *mia*)	10–20
mia1-3 × oda2	MIA complex; ODA	Beat at very low beat frequency (more severe than *mia*)	10–20
mia1-1 × oda6	MIA complex; ODA	Beat at very low beat frequency (more severe than *mia*)	10–20
mia1-1 × pf4	MIA complex; PP2A phosphatase	Beat at low beat frequency (more severe than *mia*)	∼30
mia1-1 × pf17	MIA complex; RS head	Nonmotile (more severe than *mia*)	N/A
mia2 × bop5-3	MIA complex; IC138 complex	Slightly jerky or smooth (some cells), slow swimming (similar to *mia*)	40–50
mia2 × ida6	MIA complex; N-DRC; dynein e	Nonmotile or sporadic twitching (more severe than *mia*)	N/A
mia2 × ida9	MIA complex; dynein c	Nonmotile or beat at very low beat frequency (more severe than *mia*)	<10
mia2 × oda6	MIA complex; ODA	Beat at very low beat frequency (more severe than *mia*)	10–20
mia2 × oda7	MIA complex; ODA	Beat at very low beat frequency (more severe than *mia*)	10–20
mia2 × pf4	MIA complex; PP2A phosphatase	Very short flagella (more severe than *mia*)	N/A
mia2 × pf17	MIA complex; RS head	Nonmotile (more severe than *mia*)	N/A

Typical beat frequencies of cells were measured at room temperature (∼25°C). When cells had no flagella, cells were kept rotating in distilled water for several hours to grow flagella. N/A, not analyzable.

complex does not solely regulate the single-headed IDAs or the ODAs.

To determine how the MIA complex contributes to regulation of dynein motor function, we used a sliding disintegration assay to measure microtubule sliding velocities in isolated axonemes (Okagaki and Kamiya, 1986). The microtubule sliding velocities of *mia1* were similar to wild type, although there was some slight variation in the different alleles. In contrast, microtubule sliding velocities of *mia2* were significantly reduced (Fig. 8). I1 dynein plays a role in control of microtubule sliding by a regulatory pathway that involves the CP, RS, and axonemal kinases and phosphatases (Fig. 1, A and B; Wirschell et al., 2007). Dynein-driven microtubule sliding is globally inhibited in isolated, paralyzed axonemes from RS mutants, such as *pf17*, and normal microtubule sliding velocity can be rescued by treating the axonemes with kinase inhibitors (Fig. 8, KI) including protein kinase inhibitor (PKI; the peptide inhibitor of PKA) and 5,6-dichloro-1-b-D-ribofuranosylbenzimidazole (DRB; the inhibitor of CK1). Surprisingly, these kinase inhibitors did not rescue the microtubule sliding velocities of *mia2*, whereas these treatments successfully rescued the microtubule sliding of *pf17*. In addition, kinase inhibitor treatment resulted in a decrease in microtubule sliding velocities in *mia1* (Fig. 8). As discussed in the next section, these results, although revealing the unexpected features of the MIA complex, are consistent with a role for the MIA complex in regulation of dyneins by a pathway that includes the CP/RS/I1 dynein phosphoregulatory mechanism.

Discussion

In this study, we addressed the hypothesis that the *MIA1* and *MIA2* genes encode proteins required for regulation of I1 dynein. Consistent with this, these genes encode conserved coiled-coil proteins FAP100 and FAP73, respectively (Fig. 2, A and B), which interact to form the MIA complex (Fig. 3 C), a novel regulator of dynein-driven ciliary/flagellar motility. The MIA complex localizes along the entire length of both flagella (Fig. 6 A), biochemically interacts with I1 dynein components (Fig. 5 C and Table S1), and is localized near the IC/LC complex–IC138 subcomplex of I1 dynein (Figs. 6 C and S2, A–C; Bower et al., 2009; Heuser et al., 2012b). In addition, I1 dynein stability

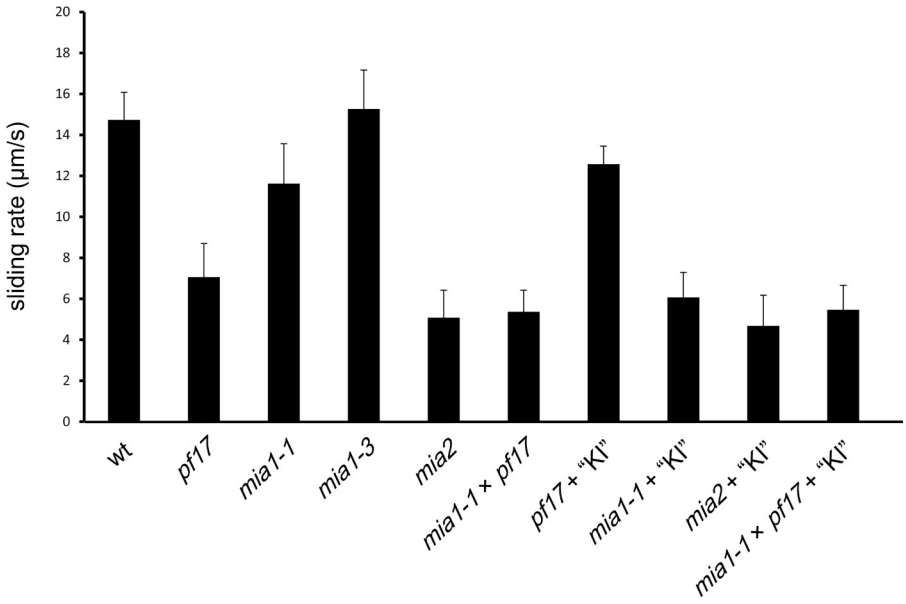

Figure 8. **Regulation of dynein-driven microtubule sliding is disrupted in the *mia* mutants.** ATP- and protease-induced microtubule sliding measurements show the characteristic sliding velocities for wild-type (wt) and *pf17* mutant axonemes. The reduced sliding velocity of *pf17* is rescued to wild-type levels by the addition of a kinase inhibitor (KI). Microtubule sliding velocities of *mia1* (*mia1-1* and *mia1-3*) are similar or only slightly reduced relative to that of wild type but greatly reduced when coupled with the *pf17* mutation (*mia1-1* × *pf17*). Microtubule sliding velocities of *mia2* axonemes are significantly reduced and are not altered by kinase inhibitor treatment (*mia2* + kinase inhibitor). Error bars show standard deviations (n = 4–36).

requires assembly of both the MIA complex and ODA (Fig. 7, A–C), consistent with the presence of a structural link between I1 dynein and ODA (Nicastro et al., 2006; Bui et al., 2012; Heuser et al., 2012b). Together, the data indicate a structural and functional interaction between I1 dynein and the MIA complex, which is required for normal ciliary motility. As illustrated in Fig. 9 (A and B), we postulate that the MIA complex physically positions the I1 dynein/IC138 (Bower et al., 2009) relative to the predicted position of the axonemal kinases and phosphatases for regulation of IC138 phosphorylation and control of ciliary waveform (King and Dutcher, 1997; Bayly et al., 2010; VanderWaal et al., 2011).

The MIA complex affects the structure and stability of I1 dynein

Among the primary results of this study was the discovery of the MIA complex. The MIA complex assembles independent of other axonemal structures: the *mia* mutants do not have defects in assembly of other major axonemal structures (Figs. 4, B and C; and 6 C), and, in turn, the MIA complex assembly is unaffected in mutants of other major axonemal complexes (Fig. 4 A). Moreover, the kinases (CK1) and phosphatases (PP2A and PP1) involved in the CP–RS–I1 regulatory pathway (Yang et al., 2000; Gokhale et al., 2009; Elam et al., 2011) are assembled at wild-type levels (Fig. 5 B). Consistent with our biochemical analyses, King and Dutcher (1997) found that only an ∼65-kD protein (FAP100), an ∼34-kD protein (FAP73), and an unknown ∼35-kD protein (also missing in *ida1*) are missing or reduced in *mia* mutant axonemes. Although *mia2* only lacks FAP73, *mia1* has defects in both FAP100 and FAP73 in the axoneme, indicating FAP100 is required for ciliary localization of FAP73 but not vice versa (Figs. 3 A and 4 A).

Cryo-ET of *mia* axonemes identified the putative location of the MIA complex on the outer DMTs. The *mia* mutant axonemes have structural defects in the region between the IC/LC complex of I1 dynein and the N-DRC (Fig. 6 C, green; and Video 5). The simplest interpretation is that the MIA complex is located adjacent to the IC/LC domain of I1 dynein, an ideal location for regulation of I1 dynein. The reduced densities further distal toward the N-DRC could be downstream structural assembly defects when the MIA complex is missing. Moreover, cryo-ET analyses clearly demonstrate that, in axonemes from the *mia* mutants, I1 dynein is specifically missing along the entire length of DMT1. ODAs are also missing from DMT1 (Hoops and Witman, 1983; Bui et al., 2009, 2012; Lin et al., 2012b). Thus, one possible explanation is that assembly or stability of I1 dynein is affected by structural interactions with both the ODA and the MIA complex. This hypothesis is supported by analyses of *mia* × *oda* double mutants, which show a reduced amount of I1 dynein relative to *oda* and *mia* single mutants (Fig. 7, B and C).

Our results indicate that the MIA complex structurally supports I1 dynein (Fig. 9, A and B). Consistent with this interpretation, I1 dynein structure is also altered in *mia* axonemes. This is illustrated by the reduced and blurred density of the I1 dynein in *mia* mutants (Figs. 6 B, 7 A, and S3). Thus, despite the assembly of I1 dynein on DMTs 2–9 in axonemes from *mia* mutants (Figs. 4, B and C; and 7, B and C), the I1 structure appears more flexible compared with that in wild type (Fig. 9 B). These observations are also consistent with our recent cryo-ET study revealing that the IC/LC complex appears to be suspended from the A tubule of outer DMTs with only a single, narrow connection (Video 1; Heuser et al., 2012b). Our observations suggest that the distal connection to the MIA complex is crucial for stable attachment of the I1 dynein IC/LC complex to the axoneme.

The MIA complex may coordinate multiple axonemal pathways for regulation of dyneins

To test whether the MIA complex functions in the signaling pathways that regulate dynein activity in vivo (e.g., in cooperation with the N-DRC for control of ODA and beat frequency [Porter, 2011] or with the CP–RS–I1 phosphorylation pathway

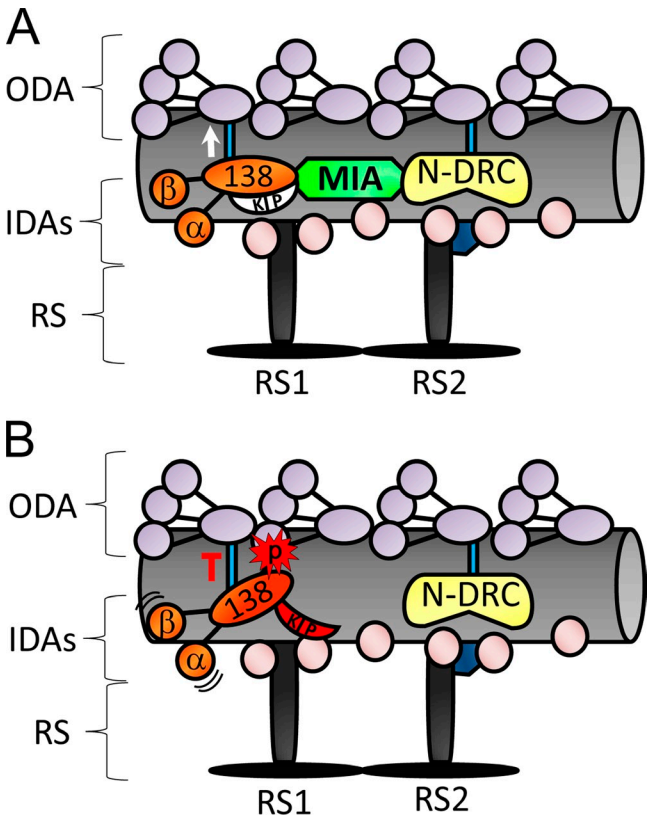

Figure 9. **Proposed model for the function of the MIA complex in regulation of I1 dynein.** (A) In wild type, the MIA complex is localized in a position to mediate signals to I1 dynein motor complex (orange). Kinases and phosphatases (white in A and red in B), such as CK1, PKA, and PP2A, are predicted to be positioned at the base of the I1 dynein complex, in position to regulate phosphorylation of the IC138 substrate of I1 dynein. (B) In the absence of the MIA complex, these signaling proteins (red) are present but may be mispositioned relative to IC138 and I1 dynein, which are flexible, resulting in hyperphosphorylated IC138 in the *mia* mutants. KIP, kinase–phosphatase complex; p, phosphorylation.

for control of I1 dynein and waveform [Wirschell et al., 2007]), we isolated and characterized double mutants between the *mia* mutants and previously characterized motility mutants (Fig. S4 and Table 1). From this analysis, we conclude that the MIA complex does not operate exclusively in any one dynein regulatory pathway. For example, the *mia* × *pf4* double mutants showed a more severe phenotype than the parent strains alone, suggesting the MIA complex and PP2A function in either separate or only partially overlapping pathways. *mia* × *ida6*, which lacks the MIA complex, several N-DRC components, and IDA e, was nearly nonmotile (Table 1). Because *mia* mutants and *ida6* alone are both slow swimmers, this result indicates that the MIA complex may function mostly independent of the N-DRC, even though the MIA complex seems to extend between I1 dynein and the N-DRC. This is consistent with the results from King and Dutcher (1997): double mutants between *mia* mutants and *pf2* or *pf3* showed severe paralyzed phenotypes. However, we cannot formally exclude a functional interaction between the MIA complex and the N-DRC. In addition, the microtubule sliding velocity in axonemes from *mia* × *pf17* double mutants is slower than in axonemes from *mia* or *pf17* alone (Fig. 8), suggesting that the MIA complex does not exclusively function in the CP–RS–I1 phosphorylation pathway (Porter and Sale, 2000; Wirschell et al., 2007). Thus, the MIA complex may operate in multiple dynein regulatory pathways that affect the activity of both I1 dynein and ODA.

From double mutant analysis, the MIA complex was clearly shown to regulate I1 dynein: doubles between *mia* mutants and the I1 dynein mutants *ida1*, *ida2*, and *bop5* showed a similar motility phenotype to *mia* alone (Fig. S4 and Table 1). In addition, the *mia* × *bop5* double mutants fail to perform phototaxis similar to the single *mia* mutants (VanderWaal et al., 2011). The *bop5* mutant is particularly informative because it only affects the assembly of the IC138 complex, whereas the remaining I1 dynein subunits assemble as in wild-type axonemes (Bower et al., 2009). Moreover, the *bop5* mutants revealed that the IC138 complex is required for control of flagellar waveform but is not required for phototaxis (VanderWaal et al., 2011). Thus, the MIA complex must have an essential role in phototactic behavior that is independent of the IC138 complex.

We observed reduced beat frequencies (~40 Hz) and slightly jerky or jerky phenotypes of the *mia* mutants (Fig. S4 and Table 1; King and Dutcher, 1997). The simplest explanation for this observation is that the MIA complex either directly or indirectly regulates ODAs because the ODAs control ciliary beat frequency (Brokaw and Kamiya, 1987). We postulate that the MIA complex affects beat frequency and ODA activity via its effects on I1 dynein. Consistent with this hypothesis, defective assembly of I1 dynein results in greatly reduced microtubule sliding velocity in isolated axonemes, suggesting a functional interaction between I1 dynein and ODAs (e.g., Kikushima, 2009; Toba et al., 2011). The functional interaction between I1 dynein and the ODAs could be mediated by the OIDLs observed by cryo-ET (Nicastro et al., 2006; Bui et al., 2012).

Possible regulatory mechanism of the MIA complex

A primary functional role of the MIA complex appears to be the regulation of I1 dynein. One model, illustrated in Fig. 9 A, indicates a direct interaction of the I1 IC138 complex (Bower et al., 2009) with the MIA complex and stable positioning of I1 dynein relative to RS1 and presumably relative to the kinase and phosphatase for IC138 (Gokhale et al., 2009; Elam et al., 2011). In agreement with this model, structural analysis of the *mia* axonemes reveals defective structure just distal to the location of the IC/LC complex (Figs. 6 C and S2, A–C) and altered structure of I1 dynein on DMTs 2–9 (Figs. 6 B, 7 A, and S3). In addition, cross-linking analysis reveals interaction between the Mia proteins and IC138 (Table S1).

Diverse evidence has revealed a correlation between the velocity of microtubule sliding and the degree of IC138 phosphorylation: increased IC138 phosphorylation correlates with inhibition of microtubule sliding (Habermacher and Sale, 1997; Wirschell et al., 2007). Thus, the microtubule sliding results of the *mia* mutants were surprising: despite increased phosphorylation of IC138 (Fig. 5 A) and deficits in structure and assembly of both FAP100 and FAP73 (Figs. 3 A, 4 A, and 6 C), microtubule sliding velocity was rapid in axonemes from *mia1* alleles

(Fig. 8). In contrast, despite smaller structural defects with only the loss of FAP73 (Figs. 3 A, 4 A, and 6 C) and increased phosphorylation of IC138, microtubule sliding in *mia2* axonemes was greatly reduced (Fig. 8). Because the in vivo motility phenotypes of *mia1* and *mia2* are similar, it was surprising to observe the large difference in microtubule sliding between *mia1* and *mia2* axonemes. In addition, we and others (King and Dutcher, 1997) observed that despite more limited axonemal structural defects, the phosphorylation state of IC138 was more excessive in *mia2* than in *mia1* (Fig. 5 A). Furthermore, addition of kinase inhibitors to *mia1* axonemes inhibited microtubule sliding, whereas neither DRB nor PKI altered or rescued microtubule sliding in *mia2* axonemes regardless of reduced IC138 phosphorylation (Fig. 8). These results reveal that the key axonemal phosphatase for IC138 is at least present in *mia* axonemes and can dephosphorylate IC138 in vitro (Fig. 5 A).

One explanation for these discrepancies is that in axonemes from the *mia* mutants, phosphorylation of IC138 is uncoupled from changes in microtubule sliding. In addition, the *mia* mutants may reveal an important in vivo regulatory mechanism that cannot be studied by the in vitro microtubule sliding assay. For example, changes in IC138 phosphorylation may be very rapid in vivo (e.g., in response to signals from the external environment required for control of waveform) and that assembly of the MIA complex is required to ensure close and efficient interaction between IC138 and axonemal kinases and phosphatases. In contrast, in in vitro assays, changes in phosphorylation may be slow. In any case, further understanding of the apparent discrepancy between live-cell motility and in vitro microtubule sliding in the *mia* mutants will require future analysis of the key, motility-related phosphoresidues in IC138 (Bower et al., 2009; VanderWaal et al., 2011).

Potential functions of the MIA complex in higher organisms

Mia proteins are well conserved from *C. reinhardtii* to mammals, suggesting the MIA complex regulates ciliary motility and/or assembly also in higher organisms. The Mia proteins each have two potential homologues in humans; CCDC37 (coiled-coil domain–containing 37) and CCDC38 for FAP100 and CCDC42A and CCDC42B for FAP73 (Fig. S5, A and B). The *CCDC42A* gene is expressed in mouse testes, and mutations in *CCDC42A* result in a failure in flagellar assembly (Yoder, B., personal communication). In addition, *CCDC37* has been recently reported to be one of five hypermethylated and down-regulated genes in human lung squamous cell carcinoma (Kwon et al., 2012). Also, *CCDC38* has been recently reported as one of 16 loci that are tightly related to normal pulmonary function (Soler Artigas et al., 2012). These studies suggest that potential Mia protein homologues have important functions in mammalian tissues/cells that bear motile cilia.

Materials and methods

Strains, DNA, and culture conditions

The strains used in this study are listed in Table S2. The *mia1-2*, *mia1-3*, and *mia1-4* strains were all produced by standard UV mutagenesis and mutant selection as described previously (Kamiya et al., 1991) and used for the first time in this study. The double mutants were constructed by standard methods (Dutcher, 1995). Cells were cultured in liquid L or Tris-acetate-phosphate medium and grown with aeration on a 14-h/10-h light/dark cycle or under constant illumination. The cDNA sequences of *C. reinhardtii* FAP100 and FAP73 have been deposited in the DNA Data Bank of Japan under accession number AB692780 and AB692781, respectively.

Preparation of flagella and axonemes

Deflagellation of *C. reinhardtii* cells was induced by treating cells with dibucaine (Witman, 1986). Flagella were collected by subsequent centrifugation. To prepare axonemes, flagella were demembranated with 0.2% Nonidet P-40 in HMDEK (30 mM Hepes, 5 mM $MgSO_4$, 1 mM DTT, 1 mM EGTA, and 50 mM potassium acetate, pH 7.4) and centrifuged to remove the membrane and matrix fraction. Flagella used for cryo-ET were isolated by the pH shock method, and axonemes were isolated after flagellar demembranation (Witman et al., 1972). Purified axonemes were resuspended in 30 mM Hepes, pH 7.4, 25 mM KCl, 5 mM $MgSO_4$, 1 mM EGTA, and 0.1 mM EDTA and processed within 24 h.

SDS-PAGE and immunoblotting

SDS-PAGE and immunoblotting were performed using standard procedures. SDS-PAGE was performed using normal acrylamide gels or 3–5% gradient gels with a 3–8 M urea gradient (Laemmli, 1970; Jarvik and Rosenbaum, 1980). Gels were stained with Coomassie brilliant blue (CBB) or silver. For immunoblotting, protein samples were separated by SDS-PAGE and transferred to a nitrocellulose membrane (Bio-Rad Laboratories). The membranes were blocked with 5% nonfat dry milk and incubated with various primary antibodies. Immunoreactive bands were detected using an HRP-conjugated secondary antibody (Bio-Rad Laboratories) and a 3,3′,5,5′-tetramethylbenzidine peroxidase substrate kit (Vector Laboratories). Antibodies used were anti-DHC1 (I1 dynein HC-α; rabbit; Myster et al., 1997), anti-IC140 (rabbit; Yang and Sale, 1998), anti-IC138 (rabbit; Hendrickson et al., 2004), anti-IC97 (rabbit; Wirschell et al., 2009), anti-IC69 (mouse; King et al., 1985), antiactin (rabbit; Kato-Minoura et al., 1997), anti-p28 (rabbit; LeDizet and Piperno, 1995a), anti-RSP1 (rabbit; Kohno et al., 2011), anti-FAP100 (rabbit; this study), anti-FAP73 (rabbit; this study), anti-PP2A B subunit (rabbit; Elam et al., 2011), anti-PP2A C subunit (mouse; Yu et al., 2001), anti-PP1 (rabbit; Yang et al., 2000), anti-CK1 (rabbit; Gokhale et al., 2009), and anti-HA clone 3F10 (rat; Roche).

Polyclonal antibody production

To produce FAP100 and FAP73 polyclonal antibodies, the coding region of *FAP100* or *FAP73* cDNA from wild-type cells was ligated into the BamHI and EcoRI sites of the pCold bacterial expression vector (Takara Bio Inc.). Protein expression was induced by IPTG. The primer pairs used to amplify the coding regions of *FAP100* and *FAP73* cDNA were FAP100-F1, 5′-CTGGATCCCATATGCCGATTTACGACGAGGCGT-3′; FAP100-R1, 5′-GAGAATTCAATCATGTCCTGCGCCAGATAC-3′;FAP73-NF1,5′-CTGGATCCCATATGGACGAGGAGGGCAGCGCGACTG-3′; and FAP73-NR1, 5′-GAGAATTCCTCAATCTCCGCGCGCGACGCCAGCGAC-3′. The BamHI and EcoRI sites are underlined. The expressed FAP100 protein contained 6×His tag sequences at its N terminus. The recombinant FAP100 protein was concentrated and collected using a Nickel column and used as the antigen. The expressed FAP73 protein contained 6×His and GST tag sequences at its N terminus. The recombinant FAP73 protein was contained in inclusion bodies, which were isolated and used as the antigen as previously described (Yamamoto et al., 2008). Rabbits were immunized with the antigens, antisera were harvested, and specific antibodies were affinity purified using recombinant proteins on immunoblot membranes.

Phenotypic rescue of *mia* mutants

For phenotypic rescue, *mia1-2* was transformed with an ∼5.4-kb HindIII–KpnI genomic fragment, which was excised from BAC 16N2 (Clemson University Genomics Institute) and cloned into the pKF19k-2 vector (Takara Bio Inc.). This fragment contained the whole *FAP100* gene. A 3×HA tag was inserted into the DraI site at the C terminus of the *FAP100* gene. The genomic fragment with the HA tag was incorporated in *mia1-2* cells by electroporation as previously described (Shimogawara et al., 1998). For phenotypic rescue of *mia2*, a modified pGenD plasmid vector was used (Fischer and Rochaix, 2001; Yamamoto et al., 2010). The coding region of *FAP73* was amplified by PCR with the primer pair FAP73-NF1, 5′-CTGGATCCCATATGGACGAGGAGGGCAGCGCGACTG-3′, and FAP73-NR1, 5′-GAGAATTCCTCAATCTCCGCGCGCGACGCCAGCGAC-3′, which

contained the recognition sites for BamHI, NdeI, and EcoRI (underlined). The NdeI–EcoRI cDNA fragment of *FAP73* was ligated into the pGenD vector and used for transformation of *mia2* cells by electroporation.

Immunoprecipitation

Immunoprecipitation under non–cross-linked conditions was performed as described previously (Yamamoto et al., 2008). In brief, the anti-FAP100, anti-FAP73, or anti-HA antibody (Roche) was attached to protein A or G beads and incubated with three times diluted 0.6 M KCl axonemal extracts at 4°C for several hours. The precipitates were washed several times, and the samples were boiled and processed for SDS-PAGE. Immunoprecipitation under cross-linked conditions was performed by the modified method of Sakato (2009). Axonemes from *mia1R* and *mia2R* were cross-linked with 5 mM EDC for 1 h at room temperature, boiled in SDS sample buffer containing 1% SDS, diluted 10 times with 1% NP-40 in TBS, and mixed with protein G beads (Santa Cruz Biotechnology, Inc.) with the anti-HA antibody. The mixture was kept rotating overnight at 4°C, washed several times, and subjected to SDS-PAGE. Precipitates were run to the length of ∼10 mm on the gels, stained briefly with CBB, and cut out for the ESI/liquid chromatography/MS/MS analysis. Non–cross-linked *mia1R* and *mia2R* axonemes were processed in the same way as controls. The proteins identified only in EDC cross-linked conditions, but not in non–cross-linked controls, are summarized as the potential Mia complex proteins in Table S1.

Immunofluorescence microscopy

Immunofluorescence microscopy and nucleoflagellar apparatus preparations were performed as previously described (Sanders and Salisbury, 1995; Taillon and Jarvik, 1995). Nucleoflagellar apparatuses were fixed with 2% formaldehyde at room temperature followed by treatment with cold acetone and methanol (−20°C). Fixed samples were stained with an anti-HA antibody (12CA5; Roche) in blocking buffer (10 mM sodium phosphate, pH 7.2, 5% normal goat serum, 5% glycerol, 1% cold fish gelatin, and 0.004% sodium azide) and then with the tetramethyl rhodamine isothiocyanate–labeled anti–mouse IgG antibody (Kirkegaard & Perry Laboratories). Images were acquired on an fluorescence microscope (Axioplan; Carl Zeiss) with a 63×/1.4 NA Plan Apochromat objective lens at room temperature (Carl Zeiss) and recorded with a charge-coupled device camera (CoolSNAP; Roper Scientific).

Microtubule sliding assay

Microtubule sliding assays were performed as described previously (Okagaki and Kamiya, 1986; Gokhale et al., 2009). Sliding was triggered by the addition of HMDEKP (10 mM Hepes, 5 mM $MgSO_4$, 1 mM DTT, 0.5 mM EDTA, 50 mM potassium acetate, and 1% of 20,000 polyethylene glycol) buffer containing 1 mM ATP and 5 µg/ml subtilisin A type VIII protease (Sigma-Aldrich) to axonemes in perfusion chambers. For inhibition experiments, we used 50 µM DRB (Enzo Life Sciences) and 100 nM PKI (Enzo Life Sciences) as kinase inhibitors. Images were recorded with a microscope (Axioplan) equipped with dark-field optics, a 40× Plan Apochromat lens, and a silicon-intensified camera (VE-1000; Dage-MTI). Video images were converted to a digital format using LabVIEW 7.1 software (National Instruments), and sliding velocity was determined manually by measuring microtubule displacement on tracings calibrated with a micrometer.

Beat frequency measurement

Flagellar beat frequency of live *C. reinhardtii* cells was determined using the method of Kamiya (2000) by measuring the vibration frequency of cell bodies with a fast Fourier transform analyzer.

Cryo-ET

Freshly isolated *C. reinhardtii* axonemes were plunge frozen and vitrified on holy grids (R2/2; 200 mesh; Quantifoil Micro Tools) as previously described (Heuser et al., 2009). In brief, the grids were glow discharged at −40 mA for 30 s and coated with 10-nm colloidal gold (Sigma-Aldrich). 3 µl of the axoneme sample and 1 µl of 10 times concentrated 10-nm colloidal gold solution were applied to the grid. Then, excess liquid was blotted away, and the grid was plunge frozen in liquid ethane that was cooled by liquid nitrogen. Grids were stored in liquid nitrogen until observed by EM.

Cryo-ET was performed on a transmission electron microscope (Tecnai F30; FEI) operated at 300 keV. Using the microscope control software SerialEM (Mastronarde, 2005), tomographic tilt series were collected from −65 to 65° with 1.5–2.5° increments using a −6- or −8-µm defocus to increase the phase contrast. Tilt series were recorded at a nominal magnification of 13,500 using a 2,000 × 2,000–pixel charge-coupled device camera (resulting in a pixel size of 1 nm; Megascan 795; Gatan) and an energy filter (GIF; Gatan) operated in zero-loss mode with 20-eV slit width. The total electron dose used for a tilt series was limited to ∼100 e/Å^2.

Tomograms showing the 3D structure of *C. reinhardtii* axonemes were reconstructed using the IMOD software package (Kremer et al., 1996) with gold fiducial marker alignment and weighted back projection. Some of the tomograms (pWT and *pf9-3/ida1*) were previously used for the analysis of other axonemal complexes (Heuser et al., 2009, 2012b; Lin et al., 2012b). Subtomogram averaging of the 96-nm axonemal repeats was performed using the Particle Estimation for Electron Tomography software (Nicastro et al., 2006) available from the Boulder Laboratory for 3D Electron Microscopy of Cell (Colorado). The University of California, San Francisco, Chimera package (Pettersen et al., 2004) was used for 3D visualization by isosurface rendering and data analysis. Resolutions of 3D structures obtained by cryo-ET were summarized in Table S3.

Computational methods

Protein domains, motifs, and families were searched using SMART (simple modular architecture research tool; European Molecular Biology Laboratory), Pfam (Wellcome Trust Sanger Institute), and Conserved Domain Database (NCBI) analyses. Coiled-coil regions were predicted by COILS version 2.2. For sequence comparisons, data were aligned using ClustalW, and the output was processed with BoxShade. Images were adjusted for contrast and brightness and assembled using Photoshop (Adobe), Paint (Windows), Illustrator (Adobe), and/or PowerPoint (Microsoft).

Online supplemental material

Fig. S1 shows the immunoblots using the affinity-purified Mia protein antibodies. Fig. S2 shows tomographic slice images obtained by cryo-ET. Fig. S3 shows the localization of the MIA complex and I1 dynein on each doublet. Fig. S4 shows the results of beat frequency analysis. Fig. S5 shows the alignment of *C. reinhardtii* Mia proteins and their potential human homologues. Table S1 lists the potential MIA complex components immunoprecipitated from EDC cross-linked axonemes. Table S2 lists *C. reinhardtii* strains used in this study. Table S3 lists resolutions obtained in cryo-ET. Video 1 shows the reconstructed axonemal repeat of pWT by cryo-ET. Video 2 shows the reconstructed axonemal repeat of *pf9-3/ida1*. Video 3 shows the reconstructed axonemal repeat of *mia1-1*. Video 4 shows the reconstructed axonemal repeat of *mia2*. Video 5 shows the reconstructed axonemal repeat of pWT with the potential location of the MIA complex in green. Online supplemental material is available at http://www.jcb.org/cgi/content/full/jcb.201211048/DC1.

This study was supported by the National Institutes of Health (GM051173 to W.S. Sale and GM083122 to D. Nicastro), grants-in-aid from the Japan Society for Promotion of Science (22570157 and 23118706 to T. Yagi and 23570189 to R. Kamiya), and a TOYOBO Biotechnology Foundation Long-term Research Grant, Uehara Memorial Foundation Postdoctoral Fellowship, and Japan Society for the Promotion of Science Postdoctoral Fellowship for Research Abroad (to R. Yamamoto).

Submitted: 7 November 2012
Accepted: 12 March 2013

References

Bayly, P.V., B.L. Lewis, P.S. Kemp, R.B. Pless, and S.K. Dutcher. 2010. Efficient spatiotemporal analysis of the flagellar waveform of *Chlamydomonas reinhardtii*. *Cytoskeleton (Hoboken)*. 67:56–69.

Bower, R., K. VanderWaal, E. O'Toole, L. Fox, C. Perrone, J. Mueller, M. Wirschell, R. Kamiya, W.S. Sale, and M.E. Porter. 2009. IC138 defines a subdomain at the base of the I1 dynein that regulates microtubule sliding and flagellar motility. *Mol. Biol. Cell*. 20:3055–3063. http://dx.doi.org/10.1091/mbc.E09-04-0277

Brokaw, C.J. 1994. Control of flagellar bending: a new agenda based on dynein diversity. *Cell Motil. Cytoskeleton*. 28:199–204. http://dx.doi.org/10.1002/cm.970280303

Brokaw, C.J. 2002. Computer simulation of flagellar movement VIII: coordination of dynein by local curvature control can generate helical bending waves. *Cell Motil. Cytoskeleton*. 53:103–124. http://dx.doi.org/10.1002/cm.10067

Brokaw, C.J. 2009. Thinking about flagellar oscillation. *Cell Motil. Cytoskeleton*. 66:425–436. http://dx.doi.org/10.1002/cm.20313

Brokaw, C.J., and R. Kamiya. 1987. Bending patterns of *Chlamydomonas* flagella: IV. Mutants with defects in inner and outer dynein arms indicate differences in dynein arm function. *Cell Motil. Cytoskeleton*. 8:68–75. http://dx.doi.org/10.1002/cm.970080110

Bui, K.H., H. Sakakibara, T. Movassagh, K. Oiwa, and T. Ishikawa. 2008. Molecular architecture of inner dynein arms in situ in *Chlamydomonas reinhardtii* flagella. *J. Cell Biol.* 183:923–932. http://dx.doi.org/10.1083/jcb.200808050

Bui, K.H., H. Sakakibara, T. Movassagh, K. Oiwa, and T. Ishikawa. 2009. Asymmetry of inner dynein arms and inter-doublet links in *Chlamydomonas* flagella. *J. Cell Biol.* 186:437–446. http://dx.doi.org/10.1083/jcb.200903082

Bui, K.H., T. Yagi, R. Yamamoto, R. Kamiya, and T. Ishikawa. 2012. Polarity and asymmetry in the arrangement of dynein and related structures in the *Chlamydomonas* axoneme. *J. Cell Biol.* 198:913–925. http://dx.doi.org/10.1083/jcb.201201120

Drummond, I.A. 2012. Cilia functions in development. *Curr. Opin. Cell Biol.* 24:24–30. http://dx.doi.org/10.1016/j.ceb.2011.12.007

Dutcher, S.K. 1995. Mating and tetrad analysis in *Chlamydomonas reinhardtii*. *Methods Cell Biol.* 47:531–540. http://dx.doi.org/10.1016/S0091-679X(08)60857-2

Dymek, E.E., T. Heuser, D. Nicastro, and E.F. Smith. 2011. The CSC is required for complete radial spoke assembly and wild-type ciliary motility. *Mol. Biol. Cell*. 22:2520–2531. http://dx.doi.org/10.1091/mbc.E11-03-0271

Elam, C.A., M. Wirschell, R. Yamamoto, L.A. Fox, K. York, R. Kamiya, S.K. Dutcher, and W.S. Sale. 2011. An axonemal PP2A B-subunit is required for PP2A localization and flagellar motility. *Cytoskeleton (Hoboken)*. 68:363–372. http://dx.doi.org/10.1002/cm.20519

Fischer, N., and J.D. Rochaix. 2001. The flanking regions of PsaD drive efficient gene expression in the nucleus of the green alga *Chlamydomonas reinhardtii*. *Mol. Genet. Genomics*. 265:888–894. http://dx.doi.org/10.1007/s004380100485

Gardner, L.C., E. O'Toole, C.A. Perrone, T. Giddings, and M.E. Porter. 1994. Components of a "dynein regulatory complex" are located at the junction between the radial spokes and the dynein arms in *Chlamydomonas* flagella. *J. Cell Biol.* 127:1311–1325. http://dx.doi.org/10.1083/jcb.127.5.1311

Gokhale, A., M. Wirschell, and W.S. Sale. 2009. Regulation of dynein-driven microtubule sliding by the axonemal protein kinase CK1 in *Chlamydomonas* flagella. *J. Cell Biol.* 186:817–824. http://dx.doi.org/10.1083/jcb.200906168

Habermacher, G., and W.S. Sale. 1997. Regulation of flagellar dynein by phosphorylation of a 138-kD inner arm dynein intermediate chain. *J. Cell Biol.* 136:167–176. http://dx.doi.org/10.1083/jcb.136.1.167

Hayashi, S., and C. Shingyoji. 2008. Mechanism of flagellar oscillation-bending-induced switching of dynein activity in elastase-treated axonemes of sea urchin sperm. *J. Cell Sci.* 121:2833–2843. http://dx.doi.org/10.1242/jcs.031195

Hayashibe, K., C. Shingyoji, and R. Kamiya. 1997. Induction of temporary beating in paralyzed flagella of *Chlamydomonas* mutants by application of external force. *Cell Motil. Cytoskeleton*. 37:232–239. http://dx.doi.org/10.1002/(SICI)1097-0169(1997)37:3<232::AID-CM5>3.0.CO;2-8

Hendrickson, T.W., C.A. Perrone, P. Griffin, K. Wuichet, J. Mueller, P. Yang, M.E. Porter, and W.S. Sale. 2004. IC138 is a WD-repeat dynein intermediate chain required for light chain assembly and regulation of flagellar bending. *Mol. Biol. Cell*. 15:5431–5442. http://dx.doi.org/10.1091/mbc.E04-08-0694

Heuser, T., M. Raytchev, J. Krell, M.E. Porter, and D. Nicastro. 2009. The dynein regulatory complex is the nexin link and a major regulatory node in cilia and flagella. *J. Cell Biol.* 187:921–933. http://dx.doi.org/10.1083/jcb.200908067

Heuser, T., E.E. Dymek, J. Lin, E.F. Smith, and D. Nicastro. 2012a. The CSC connects three major axonemal complexes involved in dynein regulation. *Mol. Biol. Cell*. 23:3143–3155. http://dx.doi.org/10.1091/mbc.E12-05-0357

Heuser, T., C.F. Barber, J. Lin, J. Krell, M. Rebesco, M.E. Porter, and D. Nicastro. 2012b. Cryoelectron tomography reveals doublet-specific structures and unique interactions in the I1 dynein. *Proc. Natl. Acad. Sci. USA*. 109:E2067–E2076. http://dx.doi.org/10.1073/pnas.1120690109

Hildebrandt, F., T. Benzing, and N. Katsanis. 2011. Ciliopathies. *N. Engl. J. Med.* 364:1533–1543. http://dx.doi.org/10.1056/NEJMra1010172

Hirokawa, N., Y. Tanaka, and Y. Okada. 2012. Cilia, KIF3 molecular motor and nodal flow. *Curr. Opin. Cell Biol.* 24:31–39. http://dx.doi.org/10.1016/j.ceb.2012.01.002

Hoops, H.J., and G.B. Witman. 1983. Outer doublet heterogeneity reveals structural polarity related to beat direction in *Chlamydomonas* flagella. *J. Cell Biol.* 97:902–908. http://dx.doi.org/10.1083/jcb.97.3.902

Jarvik, J.W., and J.L. Rosenbaum. 1980. Oversized flagellar membrane protein in paralyzed mutants of *Chlamydomonas reinhardtii*. *J. Cell Biol.* 85:258–272. http://dx.doi.org/10.1083/jcb.85.2.258

Kamiya, R. 2000. Analysis of cell vibration for assessing axonemal motility in *Chlamydomonas*. *Methods*. 22:383–387. http://dx.doi.org/10.1006/meth.2000.1090

Kamiya, R. 2002. Functional diversity of axonemal dyneins as studied in *Chlamydomonas* mutants. *Int. Rev. Cytol.* 219:115–155. http://dx.doi.org/10.1016/S0074-7696(02)19012-7

Kamiya, R., E. Kurimoto, and E. Muto. 1991. Two types of *Chlamydomonas* flagellar mutants missing different components of inner-arm dynein. *J. Cell Biol.* 112:441–447. http://dx.doi.org/10.1083/jcb.112.3.441

Kato-Minoura, T., M. Hirono, and R. Kamiya. 1997. *Chlamydomonas* inner-arm dynein mutant, *ida5*, has a mutation in an actin-encoding gene. *J. Cell Biol.* 137:649–656. http://dx.doi.org/10.1083/jcb.137.3.649

Kikushima, K. 2009. Central pair apparatus enhances outer-arm dynein activities through regulation of inner-arm dyneins. *Cell Motil. Cytoskeleton*. 66:272–280. http://dx.doi.org/10.1002/cm.20355

Kim, K.S., S. Kustu, and W. Inwood. 2006. Natural history of transposition in the green alga *Chlamydomonas reinhardtii*: use of the AMT4 locus as an experimental system. *Genetics*. 173:2005–2019. http://dx.doi.org/10.1534/genetics.106.058263

King, S.J., and S.K. Dutcher. 1997. Phosphoregulation of an inner dynein arm complex in *Chlamydomonas reinhardtii* is altered in phototactic mutant strains. *J. Cell Biol.* 136:177–191. http://dx.doi.org/10.1083/jcb.136.1.177

King, S.M., and R. Kamiya. 2009. Axonemal dyneins: Assembly, structure, and force generation. *In* The *Chlamydomonas* Sourcebook: Cell Motility and Behavior. Vol. 3. G.B. Witman, editor. Academic Press, Kidlington, Oxford. 131–208.

King, S.M., T. Otter, and G.B. Witman. 1985. Characterization of monoclonal antibodies against *Chlamydomonas* flagellar dyneins by high-resolution protein blotting. *Proc. Natl. Acad. Sci. USA*. 82:4717–4721. http://dx.doi.org/10.1073/pnas.82.14.4717

Kohno, T., K. Wakabayashi, D.R. Diener, J.L. Rosenbaum, and R. Kamiya. 2011. Subunit interactions within the *Chlamydomonas* flagellar spoke-head. *Cytoskeleton (Hoboken)*. 68:237–246. http://dx.doi.org/10.1002/cm.20507

Kotani, N., H. Sakakibara, S.A. Burgess, H. Kojima, and K. Oiwa. 2007. Mechanical properties of inner-arm dynein-f (dynein I1) studied with *in vitro* motility assays. *Biophys. J.* 93:886–894. http://dx.doi.org/10.1529/biophysj.106.101964

Kremer, J.R., D.N. Mastronarde, and J.R. McIntosh. 1996. Computer visualization of three-dimensional image data using IMOD. *J. Struct. Biol.* 116:71–76. http://dx.doi.org/10.1006/jsbi.1996.0013

Kwon, Y.J., S.J. Lee, J.S. Koh, S.H. Kim, H.W. Lee, M.C. Kang, J.B. Bae, Y.J. Kim, and J.H. Park. 2012. Genome-wide analysis of DNA methylation and the gene expression change in lung cancer. *J. Thorac. Oncol.* 7:20–33. http://dx.doi.org/10.1097/JTO.0b013e3182307f62

Laemmli, U.K. 1970. Cleavage of structural proteins during the assembly of the head of bacteriophage T4. *Nature*. 227:680–685. http://dx.doi.org/10.1038/227680a0

LeDizet, M., and G. Piperno. 1995a. The light chain p28 associates with a subset of inner dynein arm heavy chains in *Chlamydomonas* axonemes. *Mol. Biol. Cell*. 6:697–711.

Lee, L. 2011. Mechanisms of mammalian ciliary motility: Insights from primary ciliary dyskinesia genetics. *Gene*. 473:57–66. http://dx.doi.org/10.1016/j.gene.2010.11.006

Lin, J., D. Tritschler, K. Song, C.F. Barber, J.S. Cobb, M.E. Porter, and D. Nicastro. 2011. Building blocks of the nexin-dynein regulatory complex in *Chlamydomonas* flagella. *J. Biol. Chem.* 286:29175–29191. http://dx.doi.org/10.1074/jbc.M111.241760

Lin, J., T. Heuser, B.I. Carbajal-González, K. Song, and D. Nicastro. 2012a. The structural heterogeneity of radial spokes in cilia and flagella is conserved. *Cytoskeleton (Hoboken)*. 69:88–100. http://dx.doi.org/10.1002/cm.21000

Lin, J., T. Heuser, K. Song, X. Fu, and D. Nicastro. 2012b. One of the nine doublet microtubules of eukaryotic flagella exhibits unique and partially conserved structures. *PLoS ONE*. 7:e46494. http://dx.doi.org/10.1371/journal.pone.0046494

Lindemann, C.B. 2011. Experimental evidence for the geometric clutch hypothesis. *Curr. Top. Dev. Biol.* 95:1–31. http://dx.doi.org/10.1016/B978-0-12-385065-2.00001-3

Lindemann, C.B., and K.A. Lesich. 2010. Flagellar and ciliary beating: the proven and the possible. *J. Cell Sci.* 123:519–528. http://dx.doi.org/10.1242/jcs.051326

Marshall, W.F. 2008. The cell biological basis of ciliary disease. *J. Cell Biol.* 180:17–21. http://dx.doi.org/10.1083/jcb.200710085

Mastronarde, D.N. 2005. Automated electron microscope tomography using robust prediction of specimen movements. *J. Struct. Biol.* 152:36–51. http://dx.doi.org/10.1016/j.jsb.2005.07.007

Mitchison, T.J., and H.M. Mitchison. 2010. Cell biology: How cilia beat. *Nature*. 463:308–309. http://dx.doi.org/10.1038/463308a

Morita, Y., and C. Shingyoji. 2004. Effects of imposed bending on microtubule sliding in sperm flagella. *Curr. Biol.* 14:2113–2118. http://dx.doi.org/10.1016/j.cub.2004.11.028

Myster, S.H., J.A. Knott, E. O'Toole, and M.E. Porter. 1997. The *Chlamydomonas* Dhc1 gene encodes a dynein heavy chain subunit required for assembly of the I1 inner arm complex. *Mol. Biol. Cell*. 8:607–620.

Nicastro, D., C. Schwartz, J. Pierson, R. Gaudette, M.E. Porter, and J.R. McIntosh. 2006. The molecular architecture of axonemes revealed by cryoelectron tomography. *Science*. 313:944–948. http://dx.doi.org/10.1126/science.1128618

Oh, E.C., and N. Katsanis. 2012. Cilia in vertebrate development and disease. *Development*. 139:443–448. http://dx.doi.org/10.1242/dev.050054

Okagaki, T., and R. Kamiya. 1986. Microtubule sliding in mutant *Chlamydomonas* axonemes devoid of outer or inner dynein arms. *J. Cell Biol.* 103:1895–1902. http://dx.doi.org/10.1083/jcb.103.5.1895

Okita, N., N. Isogai, M. Hirono, R. Kamiya, and K. Yoshimura. 2005. Phototactic activity in *Chlamydomonas* 'non-phototactic' mutants deficient in Ca2+-dependent control of flagellar dominance or in inner-arm dynein. *J. Cell Sci.* 118:529–537. http://dx.doi.org/10.1242/jcs.01633

Pazour, G.J., N. Agrin, J. Leszyk, and G.B. Witman. 2005. Proteomic analysis of a eukaryotic cilium. *J. Cell Biol.* 170:103–113. http://dx.doi.org/10.1083/jcb.200504008

Pettersen, E.F., T.D. Goddard, C.C. Huang, G.S. Couch, D.M. Greenblatt, E.C. Meng, and T.E. Ferrin. 2004. UCSF Chimera—a visualization system for exploratory research and analysis. *J. Comput. Chem.* 25:1605–1612. http://dx.doi.org/10.1002/jcc.20084

Pigino, G., K.H. Bui, A. Maheshwari, P. Lupetti, D. Diener, and T. Ishikawa. 2011. Cryoelectron tomography of radial spokes in cilia and flagella. *J. Cell Biol.* 195:673–687. http://dx.doi.org/10.1083/jcb.201106125

Piperno, G. 1995. Regulation of dynein activity within *Chlamydomonas* flagella. *Cell Motil. Cytoskeleton*. 32:103–105. http://dx.doi.org/10.1002/cm.970320206

Porter, M.E. 2011. Flagellar motility and the dynein regulatory complex. *In* Dyneins: Structure, Biology and Disease. S.M. King, editor. Academic Press, Amsterdam/Boston. 337–365.

Porter, M.E., and W.S. Sale. 2000. The 9 + 2 axoneme anchors multiple inner arm dyneins and a network of kinases and phosphatases that control motility. *J. Cell Biol.* 151:F37–F42. http://dx.doi.org/10.1083/jcb.151.5.F37

Porter, M.E., J. Power, and S.K. Dutcher. 1992. Extragenic suppressors of paralyzed flagellar mutations in *Chlamydomonas reinhardtii* identify loci that alter the inner dynein arms. *J. Cell Biol.* 118:1163–1176. http://dx.doi.org/10.1083/jcb.118.5.1163

Roy, S. 2009. The motile cilium in development and disease: emerging new insights. *Bioessays*. 31:694–699. http://dx.doi.org/10.1002/bies.200900031

Sakato, M. 2009. Crosslinking methods purification and analysis of crosslinked dynein products. *Methods Cell Biol.* 91:161–171. http://dx.doi.org/10.1016/S0091-679X(08)91010-4

Sanders, M.A., and J.L. Salisbury. 1995. Immunofluorescence microscopy of cilia and flagella. *Methods Cell Biol.* 47:163–169. http://dx.doi.org/10.1016/S0091-679X(08)60805-5

Satir, P., and S.T. Christensen. 2007. Overview of structure and function of mammalian cilia. *Annu. Rev. Physiol.* 69:377–400. http://dx.doi.org/10.1146/annurev.physiol.69.040705.141236

Shimogawara, K., S. Fujiwara, A. Grossman, and H. Usuda. 1998. High-efficiency transformation of *Chlamydomonas reinhardtii* by electroporation. *Genetics*. 148:1821–1828.

Shingyoji, C., H. Higuchi, M. Yoshimura, E. Katayama, and T. Yanagida. 1998. Dynein arms are oscillating force generators. *Nature*. 393:711–714. http://dx.doi.org/10.1038/31520

Smith, E.F. 2002. Regulation of flagellar dynein by the axonemal central apparatus. *Cell Motil. Cytoskeleton*. 52:33–42. http://dx.doi.org/10.1002/cm.10031

Smith, E.F., and R. Rohatgi. 2011. Cilia 2010: the surprise organelle of the decade. *Sci. Signal.* 4:mr1. http://dx.doi.org/10.1126/scisignal.4155mr1

Smith, E.F., and W.S. Sale. 1992. Regulation of dynein-driven microtubule sliding by the radial spokes in flagella. *Science*. 257:1557–1559. http://dx.doi.org/10.1126/science.1387971

Smith, E.F., and P. Yang. 2004. The radial spokes and central apparatus: mechano-chemical transducers that regulate flagellar motility. *Cell Motil. Cytoskeleton*. 57:8–17. http://dx.doi.org/10.1002/cm.10155

Soler Artigas, M., L.V. Wain, and M.D. Tobin. 2012. Genome-wide association studies in lung disease. *Thorax*. 67:271–273. http://dx.doi.org/10.1136/thoraxjnl-2011-200724

Taillon, B.E., and J.W. Jarvik. 1995. Release of the cytoskeleton and flagellar apparatus from *Chlamydomonas. Methods Cell Biol.* 47:307–313. http://dx.doi.org/10.1016/S0091-679X(08)60824-9

Toba, S., L.A. Fox, H. Sakakibara, M.E. Porter, K. Oiwa, and W.S. Sale. 2011. Distinct roles of 1alpha and 1beta heavy chains of the inner arm dynein I1 of *Chlamydomonas* flagella. *Mol. Biol. Cell*. 22:342–353. http://dx.doi.org/10.1091/mbc.E10-10-0806

VanderWaal, K.E., R. Yamamoto, K. Wakabayashi, L. Fox, R. Kamiya, S.K. Dutcher, P.V. Bayly, W.S. Sale, and M.E. Porter. 2011. bop5 mutations reveal new roles for the IC138 phosphoprotein in the regulation of flagellar motility and asymmetric waveforms. *Mol. Biol. Cell*. 22:2862–2874. http://dx.doi.org/10.1091/mbc.E11-03-0270

Wirschell, M., T. Hendrickson, and W.S. Sale. 2007. Keeping an eye on I1: I1 dynein as a model for flagellar dynein assembly and regulation. *Cell Motil. Cytoskeleton*. 64:569–579. http://dx.doi.org/10.1002/cm.20211

Wirschell, M., C. Yang, P. Yang, L. Fox, H.A. Yanagisawa, R. Kamiya, G.B. Witman, M.E. Porter, and W.S. Sale. 2009. IC97 is a novel intermediate chain of I1 dynein that interacts with tubulin and regulates interdoublet sliding. *Mol. Biol. Cell*. 20:3044–3054. http://dx.doi.org/10.1091/mbc.E09-04-0276

Witman, G.B. 1986. Isolation of *Chlamydomonas* flagella and flagellar axonemes. *Methods Enzymol.* 134:280–290. http://dx.doi.org/10.1016/0076-6879(86)34096-5

Witman, G.B., K. Carlson, J. Berliner, and J.L. Rosenbaum. 1972. *Chlamydomonas* flagella. I. Isolation and electrophoretic analysis of microtubules, matrix, membranes, and mastigonemes. *J. Cell Biol.* 54:507–539. http://dx.doi.org/10.1083/jcb.54.3.507

Yagi, T., S. Kamimura, and R. Kamiya. 1994. Nanometer scale vibration in mutant axonemes of *Chlamydomonas. Cell Motil. Cytoskeleton*. 29:177–185. http://dx.doi.org/10.1002/cm.970290209

Yamamoto, R., H.A. Yanagisawa, T. Yagi, and R. Kamiya. 2008. Novel 44-kilodalton subunit of axonemal Dynein conserved from *Chlamydomonas* to mammals. *Eukaryot. Cell*. 7:154–161. http://dx.doi.org/10.1128/EC.00341-07

Yamamoto, R., M. Hirono, and R. Kamiya. 2010. Discrete PIH proteins function in the cytoplasmic preassembly of different subsets of axonemal dyneins. *J. Cell Biol.* 190:65–71. http://dx.doi.org/10.1083/jcb.201002081

Yang, P., and W.S. Sale. 1998. The Mr 140,000 intermediate chain of *Chlamydomonas* flagellar inner arm dynein is a WD-repeat protein implicated in dynein arm anchoring. *Mol. Biol. Cell*. 9:3335–3349.

Yang, P., L. Fox, R.J. Colbran, and W.S. Sale. 2000. Protein phosphatases PP1 and PP2A are located in distinct positions in the *Chlamydomonas* flagellar axoneme. *J. Cell Sci.* 113:91–102.

Yu, X.X., X. Du, C.S. Moreno, R.E. Green, E. Ogris, Q. Feng, L. Chou, M.J. McQuoid, and D.C. Pallas. 2001. Methylation of the protein phosphatase 2A catalytic subunit is essential for association of Balpha regulatory subunit but not SG2NA, striatin, or polyomavirus middle tumor antigen. *Mol. Biol. Cell*. 12:185–199.